GRAĐEVINSKI MATERIJALI I KONSTRUKCIJE

Volume 68
June 2025
ISSN 2217-8139 (Print)
ISSN 2335-0229 (Online)
UDK: 06.055.2:62-03+620.1+624.001.5(497.1)=861

BUILDING MATERIALS AND STRUCTURES

2

Society for Materials and Structures Testing of Serbia
University of Belgrade Faculty of Civil Engineering
Association of Structural Engineers of Serbia

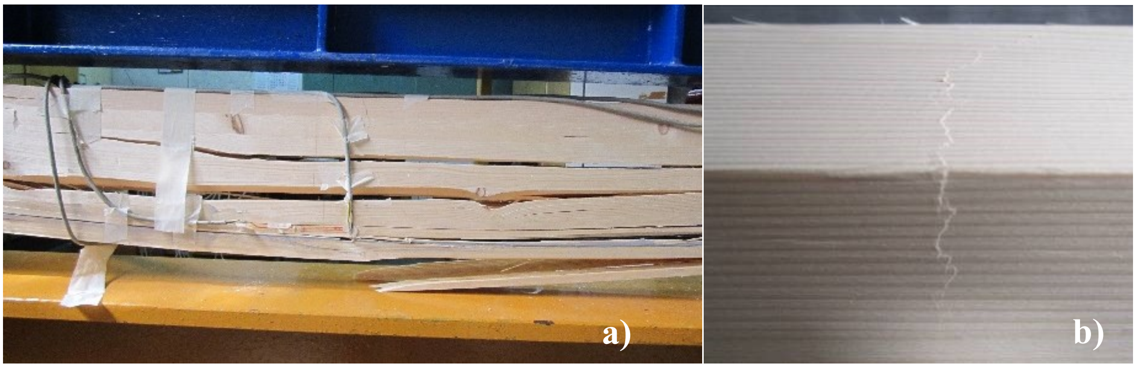

GRAĐEVINSKI MATERIJALI I KONSTRUKCIJE

BUILDING MATERIALS AND STRUCTURES

ISSN 2217-8139 (PRINT)
ISSN 2335-0229 (Online)

VOLUME 68(2)
June 2025

CONTENTS

GRAĐEVINSKI MATERIJALI I KONSTRUKCIJE

BUILDING MATERIALS AND STRUCTURES

ISSN 2217-8139 (PRINT)
ISSN 2335-0229 (Online)

VOLUME 68(2)
June 2025

Aims and scope

Building Materials and Structures aims at providing an international forum for communication and dissemination of innovative research and application in the field of building materials and structures. Journal publishes papers on the characterization of building materials properties, their technologies and modeling. In the area of structural engineering Journal publishes papers dealing with new developments in application of structural mechanics principles and digital technologies for the analysis and design of structures, as well as on the application and skillful use of novel building materials and technologies.

The scope of Building Materials and Structures encompasses, but is not restricted to, the following areas: conventional and non-conventional building materials, recycled materials, smart materials such as nanomaterials and bio-inspired materials, infrastructure engineering, earthquake engineering, wind engineering, fire engineering, blast engineering, structural reliability and integrity, life cycle assessment, structural optimization, structural health monitoring, digital design methods, data-driven analysis methods, experimental methods, performance-based design, innovative construction technologies, and value engineering.

Publishers Society for Materials and Structures Testing of Serbia**,** Belgrade, Serbia, veb sajt: www.dimk.rs
University of Belgrade Faculty of Civil Engineering, Belgrade, Serbia, www.grf.bg.ac.rs
Association of Structural Engineers of Serbia, Belgrade, Serbia, dgks.grf.bg.ac.rs

Print Razvojno istraživački centar grafičkog inženjerstva, Belgrade, Serbia

Edition quarterly

Peer reviewed journal

Journal homepage www.dimk.rs

Cover Failure mode of reinforced beams: a) global tensile failure in laminations above CFRP plate; b) compression wrinkles in top laminations from *Numerical modelling of CFRP internally reinforced glulam beams* by Ivan Glišović, Marija Todorović*,* Nađa Simović and Marko Pavlović

Financial support Ministry of Education, Science and Technological Development of Republic of Serbia
University of Belgrade Faculty of Civil Engineering
Institute for testing of materials-IMS Institute, Belgrade
Faculty of Technical Sciences, University of Novi Sad, Department of Civil Engineering
Serbian Chamber of Engineers

CIP - Каталогизација у публикацији
Народна библиотека Србије, Београд

620.1

GRAĐEVINSKI materijali i konstrukcije = Building materials and structures / editor-in-chief Snežana Marinković
. - God. 54, br. 3 (2011)- . - Belgrade : Society for Materials and Structures Testing of Serbia : University of Belgrade, Faculty of Civil Engineering : Association of Structural Engineers of Serbia, 2011- (Belgrade : Razvojno istraživački centar grafičkog inženjerstva). - 30 cm

Tromesečno. - Je nastavak: Materijali i konstrukcije
= ISSN 0543-0798. - Drugo izdanje na drugom medijumu:
Građevinski materijali i konstrukcije (Online) = ISSN 2335-0229
ISSN 2217-8139 = Građevinski materijali i konstrukcije
COBISS.SR-ID 188695820

Građevinski materijali i konstrukcije
Building Materials and Structures

journal homepage: www.dimk.rs

https://doi.org/10.5937/GRMK2500002G UDK: 624.9.011.1:678.1:519.87
620.1:519.87

Original scientific paper

Numerical modelling of CFRP internally reinforced glulam beams

Ivan Glišović[1)], Marija Todorović[*1)], Nađa Simović[1)], Marko Pavlović[2)]

[1)] *Faculty of Civil Engineering, University of Belgrade, Belgrade, Serbia*
[2)] *Delft University of Technology, Delft,Netherlands*

Article history

Received: 03 March 2025
Received in revised form: 09 April 2025
Accepted: 14 April 2025
Available online: 15 May 2025

Keywords

Glulam,
CFRP plate,
FEM,
anisotropic plasticity,
progressive damage

ABSTRACT

Numerous studies have proven that timber structures can be effectively reinforced using fibre-reinforced polymer (FRP) composites. In this paper a nonlinear finite element model was developed to predict bending behaviour of glulam beams reinforced with carbon fibre reinforced polymer (CFRP) plates strategically located in the tension zone between the bottom two laminations. The developed model was validated through comparison with the results of experimental tests for both unreinforced and reinforced beams. To accurately simulate the mechanical behaviour of hybrid glulam-CFRP members, suitable constitutive relations for each material were utilised in the model. The theory of anisotropic plasticity was implemented to include plastic behaviour of timber laminations in the compression zone. The Hill's criterion for orthotropic materials was used as a condition for transition to the plastic state. The progressive damage model was introduced to effectively simulate softening behaviour of timber in tension. The FEM results have shown excellent agreement with the experimental results. Nonlinear behaviour of glulam beams internally reinforced with CFRP was achieved in the numerical analysis, demonstrating the accuracy of developed model past the linear-elastic range.

1 Introduction

Timber structures represent a popular choice in today's construction industry as a sustainable solution which has a positive impact on the environment and the experience of occupants. Accurate prediction of timber structural elements behaviour under different loading conditions is difficult due to variability in stiffness and strength properties of wood, which is a consequence of natural defects and discontinuities. Nowadays, there is an increasing tendency to eliminate those uncertainties and improve mechanical performance of timber structures. There are numerous studies proving the effectiveness of strengthening or reinforcing timber members using fibre-reinforced polymer (FRP) composites [1-9]. Features such as high stiffness and strength, low weight, good durability (no corrosion), electromagnetic neutrality, availability in different shapes and flexibility make FRP composites convenient for reinforcement of timber structures. FRP reinforcement placed in tension zone of timber beams may produce significant improvements in stiffness and ultimate load capacity. Two most commonly used FRPs are glass (GFRP) and carbon (CFRP).

As experimental research requires resources which make it a time-consuming and expensive, numerical models can be a time-saving and cost-effective solution. Additionally, numerical models can be used to further analyse and optimise existing experimentally obtained data. Some published works have already numerically investigated the performance of FRP-reinforced timber members in different arrangements. Nowak et al. [10] analysed CFRP strips inserted vertically and horizontally into the cross-section of timber beams by considering two behaviour models of wood: elastic and elastic-ideally plastic model. Although satisfactory agreement was obtained between experimental and numerical results, authors concluded that further research is needed in order to better describe the behaviour of timber beams under bending. Szczecina [11] studied glulam beams strengthened with CFRP plates in four-point bending test by considering different material models for timber (orthotropic linear-elastic and orthotropic elasto-plastic) and different definitions of cross-section of glulam beams (modelling of the whole section or division into laminations). FEM results showed that linear-elastic model is valid only for relatively small values of mid-span deflection and that division of cross-section into laminations has no significant impact. Raftery and Harte [12] discuss the development of a nonlinear finite element model that has the capability to predict the mechanical behaviour of low-grade glued laminated timber reinforced in flexure with GFRP plates. The model incorporates anisotropic plasticity theory for timber laminations in the compression zone of the glulam with the

* Corresponding author:
E-mail address: todorovicm@grf.bg.ac.rs

failure model based on the maximum stress criterion. Strong agreement is found between the simulated load-deflection behaviour and the experimental results of unreinforced and GFRP plate reinforced glulam. The model predicts the nonlinear performance of the reinforced beams with good accuracy with satisfactory results achieved in relation to elastic stiffness and ultimate moment capacity. Khelifa et al. [13] focused on the flexural behaviour of solid timber beams externally reinforced using CFRP. Elasto-plastic behaviour with damage effect was assumed for timber material. The conclusion was that the flexural behaviour of solid timber beams can be modelled through a local approach based on the coupling of orthotropic elasticity, Hill's plasticity anisotropic quadratic criterion and cohesive model.D. Harrach et al. [14] conducted reliability-based analysis by creating probabilistic nonlinear finite element models of glulam beams reinforced with CFRP plate as well as unreinforced glulam beam under bending. Properties of timber material are considered as random variables following a normal distribution with mean value and standard deviation. This research has successfully given a deep understanding of how uncertainties play a crucial role on the deformations and stresses of considered FE models. Based on these studies and results it has become clear that accurate definition of material behaviour is the most important part of modelling.

This paper presents numerical analysis of bending behaviour of glulam beams reinforced with CFRP plates strategically located in the tension zone between the bottom two laminations, performed with the aim of determining accurate stress-strain state. A nonlinear three-dimensional finite element model was developed using software package Abaqus.The theory of anisotropic plasticity was implemented to include plastic behaviour of timber laminations in the compression zone with the Hill's criterion for orthotropic materials as a condition for transition to the plastic state. Moreover, in order to improve existing FEM models, the progressive damage model was introduced to effectively simulate softening behaviour of timber in tension. Numerical model was validated through comparison of the predicted load-deflection behaviour, stiffness, maximum load and strain profile distribution with experimentally obtained data.

2 Materials and methods

2.1 Experimental research

The experimental testing was performed at the Laboratory of Structures, Faculty of Civil Engineering, University of Belgrade conducted the experimental testing. Eight unreinforced control glulam beams (Series A) and five glulam beams reinforced with CFRP plates incorporated in between two last laminations (Series F) were tested. These tests were a part of a larger study on reinforcement possibilities of glulam beams using FRP materials [6].

Geometry of the test series is shown in Fig. 1. Tested glulam beams were made from spruce timber classified in the strength class C24 according to EN 338 [15].Dimensions of glulam beams were 80 mm width × 210 mm height × 4000 mm length. Each beam was composed of seven 30 mm thick laminations. Reinforced beams were manufactured with six laminations, and the seventh one was added after the reinforcement was placed and proper bond was established between the reinforcement and the beam. Unidirectional CFRP plate (Sika CarboDur S613) was used as reinforcement with dimensions of 1.3 mm thickness × 60 mm width×4000 mm length. The manufacturer provided following mechanical properties: modulus of elasticity 165 GPa and tensile strength 2800 MPa [16]. The plate was bonded using epoxy adhesive (Sikadur-330). Bonded-in reinforcement is associated with improved fire protection, as well as being visually more acceptable in comparison to external reinforcement. In addition, the possibility of premature delamination is significantly reduced when reinforcement is placed internally due to a greater bond area [4].

Guidelines given in EN 408 [17] were followed during the testing in four-point bending configuration presented in Fig. 2. The beams were simply supported over 3780 mm span with the load applied in thirds of the span. Loading was stroke-controlled and it gradually increased until failure using a hydraulic jack. During testing, load was transformed from one load point to two load points using a steel beam. Roller bearings were used as supports and at the load application points. Steel plates were positioned at the load application and support positions to minimize the effects of local indentation. Moreover, lateral bracing was provided to prevent lateral instability of the beams. Load was recorded

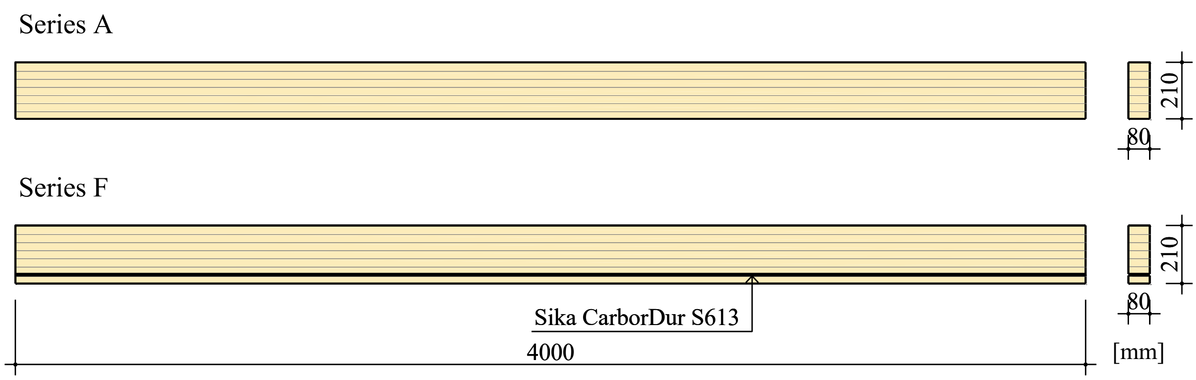

Fig. 1. Unreinforced (Series A) and reinforced beam (Series F)

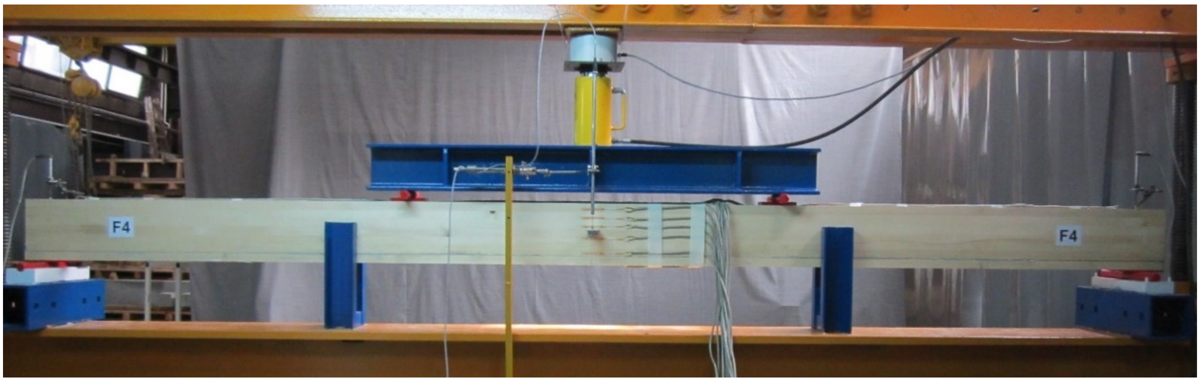

Fig. 2. Test layout

with a compression load cell, while deflection at mid-span was measured using linear variable differential transducers (LVDTs). Strains were measured using strain gauges at various locations throughout the beam's height at mid-span. All readings from loading cell, LVDTs and strain gauges were recorded using a computerized data acquisition system.

2.2 Numerical modelling

2.2.1 Model description

FEM software package Abaqus [18] was used for modelling of tested beams. As the experimental set-up was symmetrical around *x*- and *y*-axis, in order to optimize calculations, symmetry constraints were introduced and only 1/4 of the beam was modelled. The support was modelled as a roller bearing, restraining only the movement in vertical direction. Steel plates that were positioned at supports and loading points were also incorporated in the model to avoid stress concentrations at these sensitive positions. Based on experimental investigation, certain simplifications have been determined for the numerical model, such as:

- Each lamination was modelled separately to account for their different compressive and tensile behaviour, as explained in material characterisation chapter;
- Perfect connection was implemented at bonding interfaces between the laminations, since no bond-line failures were observed during experimental testing;
- A perfectly bonded connection was assumed to exist between timber and reinforcement as bonds of high quality were established during the experimental testing;
- No slip was included at the interface between steel plates and the timber surface.

Glulam beams were modelled using 8-node solid elements with reduced integration (C3D8R), CFRP plates using 4-node membrane elements with reduced integration (M3D4R) and steel plates using 4-node shell elements (S4), all available in Abaqus [18]. A mesh discretisation study was conducted to determine the finite element sizes. Two finite elements were adopted through the thickness of each timber lamination and one element through the thickness of CFRP plate. Finer mesh was generated for laminations adjacent to the CFRP plate, where stress transfer from CFRP plate to glulam occurs. Fig. 3 illustrates the adopted finite element mesh. The numerical analysis was performed using the Dynamic/Explicit solver. A series of vertical displacement increments were applied across the width of the beam until failure. As geometrical nonlinearities were considered, equilibrium equations are always formulated in the current configuration using current nodal positions, with the update of the finite element stiffness matrix at each increment [19].

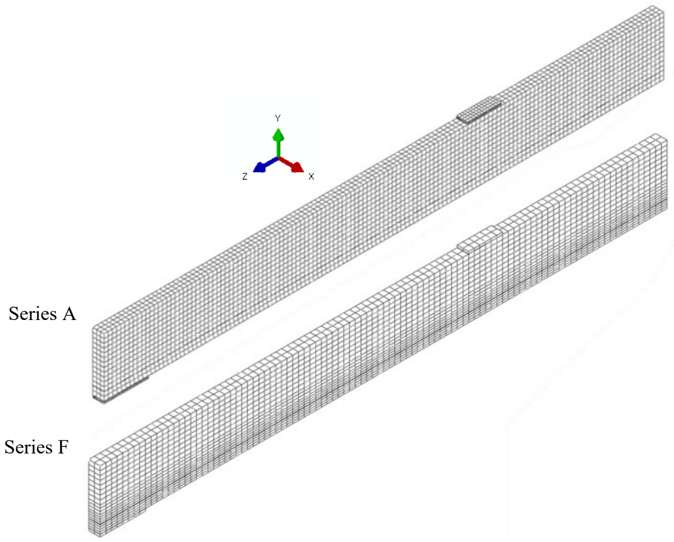

Fig. 3. Mesh discretisation for unreinforced (Series A) and reinforced (Series F) beams

2.2.2 Material characterisation

Accuracy of material modelling is of utmost importance in FEM modelling. Material input parameters for the finite element model were determined from material characterisation testing, known relationships and published data available in the constitutive relations for each material were utilised.

As timber is considered to be an orthotropic material, three main anatomical directions were assigned to the three principal axes (Fig.4).The behaviour of timber in the elastic region was described using nine independent engineering constants (three moduli of elasticity, three shear moduli and three Poisson's ratios).

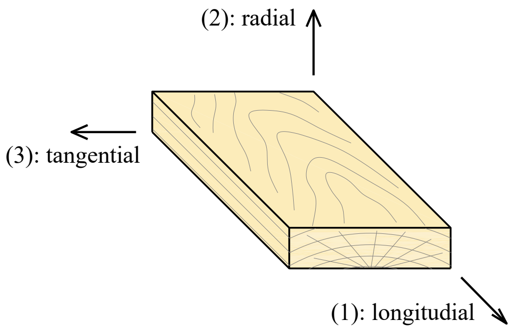

Fig. 4. Local coordinate system for timber

CFRP composite was considered to be a liner-elastic anisotropic material with transverse isotropy. Steel was treated as linear-elastic isotropic material.

Properties of each material were assumed to be independent of loading rates. Effects of environment, such as moisture and temperature, on the behaviour of timber were not taken into consideration. The material parameters of timber, CFRP plate and steel used for numerical simulations are presented in Table 1.

Table 1.Material parameters of timber and CFRP plates used in numerical modelling

	Timber	CFRP plate	Steel
Modulus of elasticity E (MPa)			
E_1	11,080	165,543	210,000
E_2	886	10,000	210,000
E_3	554	10,000	210,000
Poisson's ratio v (-)			
v_{12}	0.37	0.3	0.3
v_{13}	0.42	0.3	0.3
v_{23}	0.47	0.03	0.3
Shear modulus G (MPa)			
G_{12}	791	5,000	-
G_{13}	744	5,000	-
G_{23}	79	1,000	-

Experimental research was performed on small specimens to obtain the modulus of elasticity of timber (E_1) in the longitudinal direction. Timber has different moduli of elasticity for tension, compression and bending, but their values are very similar and for practical purposes assumed to be identical. General relationships as expressed in [20] were used to calculate the moduli in the transverse directions and shear planes, as well as Poisson's ratios. The elastic parameters for CFRP plate were adopted based on experimental tests (E_1) as well as values given in [21]. The properties in the plate thickness direction were taken the same as those in the transverse direction.

An important part of the numerical procedure is the selection of the most adequate timber strength values. Due to stress distribution effect in timber flexural members, tensile stress at failure is greater in bending than in axial tension. Hence, ultimate tensile stress was assumed to be equal to bending strength ($f_{t,0}$ = f_m =42.5 MPa) obtained from bending tests, which were conducted on small timber specimens taking into account size effect. The ultimate tensile stress will effectively be increased with addition of CFRP plate [6]. Horizontal reinforcement in tension zone acts as a bridge over timber defects and damages, and contributes to tensile capacity of the glulam beam. Experimental research has shown that the average extreme tensile strain at failure increased for reinforced over the unreinforced beams. Large strains at failure indicate large stresses at failure. Since no information was available for tensile strength in bending of reinforced timber, numerical procedure was modified to account for enhancement of bending strength using a modification factor. In this case, according to the ultimate tensile strain data, modification factor was taken as 1.25, therefore $f_{t,0,mod}$= 53 MPa.

Stress-strain relationship model for timber is presented in Fig. 5 where elastic-perfectly plastic behaviour was adopted for compression (negative part of the diagram) and elastic-softening behaviour for tension (positive part of the diagram).Exponential softening model was used to describe the softening behaviour of timber under tension [22]. Unmodified timber stress-strain curve was implemented for the bottom lamination. However, as the reinforcement influenced the laminations above it, modified stress-strain curve was adopted, as presented in Fig. 5.

Yield stresses of timber were considered to be equal to its compressive and shear strengths in various directions. These properties were estimated based onconducted material tests and available data for spruce timber in literature. The assumed yield points are shown in Table 2.

Table 2. Yield points assumed for numerical analysis

Yield stress (MPa)							
$\bar{\sigma}_{11}$	$\bar{\sigma}_{22}$	$\bar{\sigma}_{33}$	$\bar{\sigma}_{12}$	$\bar{\sigma}_{13}$	$\bar{\sigma}_{23}$	σ^0	τ^0
36.3	5.0	5.0	6.1	6.1	3.0	36.3	21.0

The theory of anisotropic plasticity was applied to include plastic mechanical behaviour of timber laminations in the compression zone. Plasticity was defined in Abaqus using yield stress and plastic strain. The Hill's criterion for orthotropic materials was used as a condition for transition to the plastic state:

$$f(\sigma)=\sqrt{F(\sigma_{22}-\sigma_{33})^2+G(\sigma_{33}-\sigma_{11})^2+H(\sigma_{11}-\sigma_{22})^2+2L\sigma_{23}^2+2M\sigma_{31}^2+2N\sigma_{12}^2} \quad (1)$$

where *F, G, H, L, M* and *N* are constants calculated based on the material strength characteristics for different directions:

$$F=\frac{(\sigma^0)^2}{2}\left(\frac{1}{\bar{\sigma}_{22}^2}+\frac{1}{\bar{\sigma}_{33}^2}-\frac{1}{\bar{\sigma}_{11}^2}\right)=\frac{1}{2}\left(\frac{1}{R_{22}^2}+\frac{1}{R_{33}^2}-\frac{1}{R_{11}^2}\right)\qquad L=\frac{3}{2}\left(\frac{\tau^0}{\bar{\sigma}_{23}^2}\right)^2=\frac{3}{2R_{23}^2}$$
$$G=\frac{(\sigma^0)^2}{2}\left(\frac{1}{\bar{\sigma}_{33}^2}+\frac{1}{\bar{\sigma}_{11}^2}-\frac{1}{\bar{\sigma}_{22}^2}\right)=\frac{1}{2}\left(\frac{1}{R_{33}^2}+\frac{1}{R_{11}^2}-\frac{1}{R_{22}^2}\right)\qquad M=\frac{3}{2}\left(\frac{\tau^0}{\bar{\sigma}_{13}^2}\right)^2=\frac{3}{2R_{13}^2}\tag{2}$$
$$H=\frac{(\sigma^0)^2}{2}\left(\frac{1}{\bar{\sigma}_{11}^2}+\frac{1}{\bar{\sigma}_{22}^2}-\frac{1}{\bar{\sigma}_{33}^2}\right)=\frac{1}{2}\left(\frac{1}{R_{11}^2}+\frac{1}{R_{22}^2}-\frac{1}{R_{33}^2}\right)\qquad N=\frac{3}{2}\left(\frac{\tau^0}{\bar{\sigma}_{12}^2}\right)^2=\frac{3}{2R_{12}^2}$$

Hill's parameters that were used in the model are:

$$R_{11}=\frac{\bar{\sigma}_{11}}{\sigma^0}=\frac{36.3}{36.3}=1\qquad R_{12}=\frac{\bar{\sigma}_{12}}{\tau^0}=\frac{6.1}{21.0}=0.29$$
$$R_{22}=\frac{\bar{\sigma}_{22}}{\sigma^0}=\frac{5.0}{36.3}=0.14\qquad R_{13}=\frac{\bar{\sigma}_{13}}{\tau^0}=\frac{6.1}{21.0}=0.29\tag{3}$$
$$R_{33}=\frac{\bar{\sigma}_{33}}{\sigma^0}=\frac{5.0}{36.3}=0.14\qquad R_{23}=\frac{\bar{\sigma}_{23}}{\tau^0}=\frac{3.0}{21.0}=0.14$$

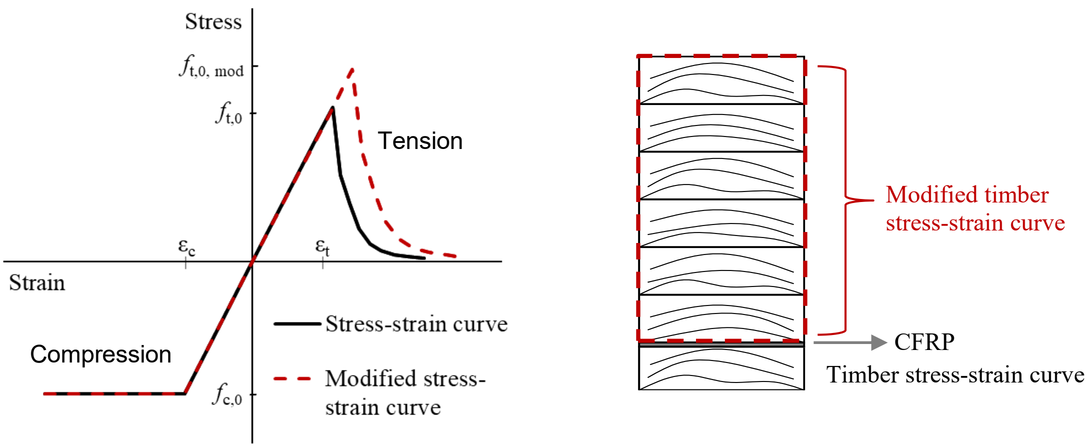

Fig. 5. Stress-strain curve for timber

For laminations in tension zone, the progressive damage model was introduced to effectively tackle the softening behaviour of timber. There are eight stress-based failure criteria or damage initiation functions proposed by Sandhaas and van de Kuilen[23]. Criterion I presents failure in tension parallel-to-grain, Criterion II –failure in compression parallel-to-grain, Criteria III–IV –failure in tension perpendicular-to-grain, Criteria V–VI– failure in compression perpendicular-to-grain and Criteria VII–VIII – shear failure. Failure Criterion I was selected to quantify damage initiation and propagation since tensile failure predominantly occurred in the experimental research. Additionally, only fracture due to tensile stress in the longitudinal direction of timber was considered. Therefore, softening behaviour and stiffness degradation in radial and tangential directions were neglected in order to optimize the calculations. The damage initiation and propagation criterion for failure in tension parallel-to-grain can be thus expressed as:

$$F_{t,0}(\sigma)=\sigma_L / f_{t,0}\leq 1\tag{4}$$

where σ_L– tensile stress parallel-to-grain of damaged material and $f_{t,0}$–tensile strength in bending.

Once a damage initiation criterion is satisfied, further loading will cause degradation of material stiffness coefficients. Reduction of stiffness coefficients is controlled by damage variables that have values between zero (undamaged state) and one (fully damaged state). Damage variable $d_{t,i}$ is expressed as:

$$d_{t,i}=1-\sigma_L / f_{t,0}\tag{5}$$

The evolution of each damage variable in the post-damage initiation phase is governed by an equivalent plastic displacement (Fig. 6). The equivalent plastic displacement for a failure mode is expressed as:

$$u_{pl}=L\,(\varepsilon_{pl}-\varepsilon_{0,pl})\tag{6}$$

where ε_{pl}– strain of damaged material, $\varepsilon_{0,pl}$– strain at the onset of damage and *L*– characteristic length of the finite element.

Damaged material is implemented as a relation of damage variable d and equivalent plastic displacement u_{pl}, as shown in Fig. 6. Damage variable d is specified directly as a tabular function of equivalent plastic displacement u_{pl}, represented by a series of points on the diagram.

3 Results and discussion

Results obtained from the numerical model were verified through the comparison with the experimental test results. The global responses of the beams in terms of load versus mid-span deflection are shown in Fig. 7.

Linear load-deflection behaviour was recorded experimentally in the case of unreinforced glulam beams (Series A), as can be seen in Fig. 7. Failure was caused by excessive tensile stresses in bottom laminations. This failure mode is generally brittle and sudden without signs of compressive plasticization at the top. Failure was mostly initiated at defects or discontinuities (e.g. knots), which were located in the zone of maximum bending moment between load application points. Behaviour predicted by the finite element model for unreinforced beams was entirely linear elastic up to failure and demonstrates good agreement with experimentally determined behaviour.

Glulam beams reinforced with CFRP plate (Series F) demonstrated significant nonlinear load-deflection behaviour (Fig. 7). The most frequent failure mechanism of these beams included two stages: local failure at timber lamination below the reinforcement and global failure above the reinforcement. After the initial linear-elastic behaviour, load resistance decreased sharply due to tensile/bending failure of the bottom lamination below the reinforcement (evident as a sudden drop in the load-deflection curve). As the reinforcement remained in position, the beams continued to carry the load in the same way as beams reinforced at the intrados surface (with reduced cross-section and increased reinforcement percentage) which resulted in nonlinear load-deflection behaviour. Load increased up to a subsequent global tensile/bending failure in laminations above the CFRP plate. Failure in the tension zone was accompanied by pronounced shear cracks that extended along the timber-reinforcement interface and/or through timber laminations above the reinforcement (Fig. 8a). Compression wrinkles were clearly visible in the top laminations, but the failure did not occur in the compression zone (Fig. 8b). Horizontal shear failure after partial cracking of timber lamination below the reinforcement. It was caused by a wood defect that manifests as tangential separation of the wood fibres along parts of the annual rings (ring shake). In addition, one beam had a premature tension failure initiated in the lamination above the reinforcement caused by a large knot. Due to the brittle nature of the timber's behaviour in tension and shear, these two beams failed suddenly, without visible warning signs before reaching ultimate load carrying capacity. The influence of different failure mechanisms of reinforced beams on the deflection values is significantly higher than on the maximum load values. The effectiveness of the reinforcement is mainly conditioned by the wood defects. A higher degree of reinforcement activation introduces nonlinearity into the global behaviour of the beams and enables less brittle failure compared to the unreinforced beams.

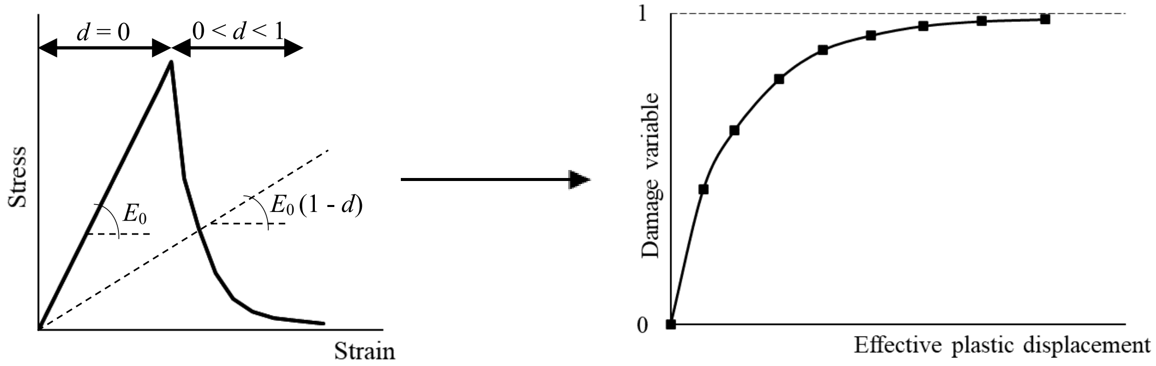

Fig. 6. Stress-strain curve transformation to damage variable-effective plastic displacement

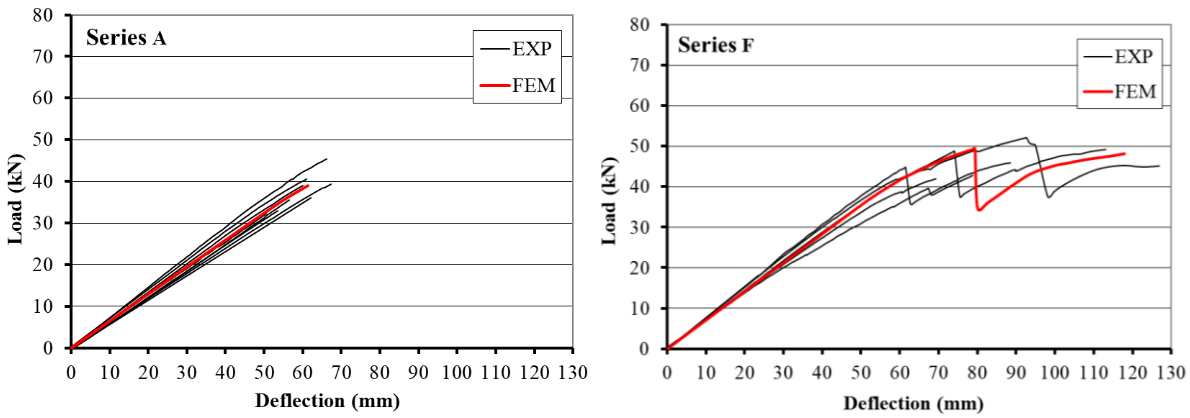

Fig. 7. Load-deflection curves for unreinforced (Series A) and reinforced (Series F) beams

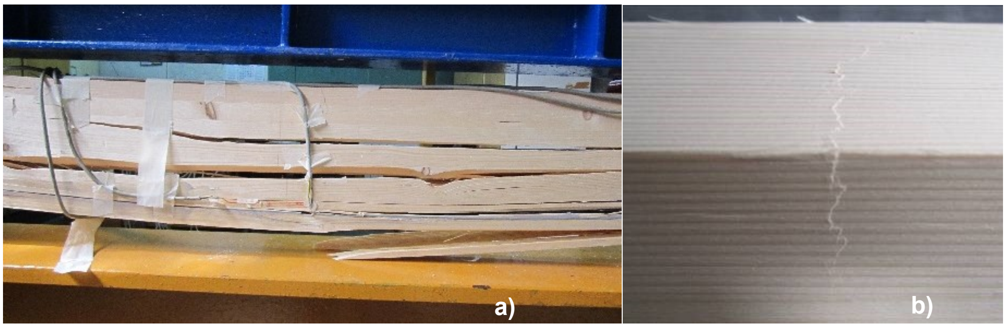

Fig. 8. Failure mode of reinforced beams: a) global tensile failure in laminations above CFRP plate; b) compression wrinkles in top laminations

FEM model of reinforced beams replicated the behaviour of experimentally tested specimens, including the failure in two stages: local failure in the timber lamination below the CFRP plate and global failure in the timber lamination above the CFRP plate. Once the first stage failure happened, the bottom lamination was excluded from the further analysis and rest of the beam continued carrying the load until the global failure. Nonlinear behaviour of beams before global failure was recorded in the numerical model, confirming the FEM model to be accurate past the linear-elastic range.

The normal stress distributions in the reinforced beam obtained from the numerical analysis are given in Figs. 9a and 10a.The area of maximum stresses, which corresponds to the bending moment diagram, can be clearly seen. In the first stage (before the failure of the timber lamination below the reinforcement), the distribution of normal stresses is almost identical in the tension and compression zones. The normal stresses increase with distance from the cross-section's centre of gravity, with the maximum normal stress occurring at the soffit of the beam. The tensile fracture in the lamination below the CFRP platewas determined by the local deformation in the area under the steel plate where the load was applied. Due to the plasticization of the compression zone, within the second stage (after the failure of the timber lamination below the reinforcement), distribution of normal stresses is not uniform. Reaching the ultimate tensile stress in the timber lamination above the reinforcement leads to the global failure of the reinforced beam.

The normal stress distributions in the CFRP plate of the reinforced beam are uniform along the entire length, as seen in Figs. 9b and 10b.The results of the numerical analysis show that the plate capacity is generally underutilized in the linear region of the beam's behaviour (first stage). After the plasticization in the compression zone (second stage), the degree of CFRP plate utilization is somewhat higher. The calculated maximum tensile stress in the plate at the ultimate load of reinforced beam was less than 40% of its tensile strength.

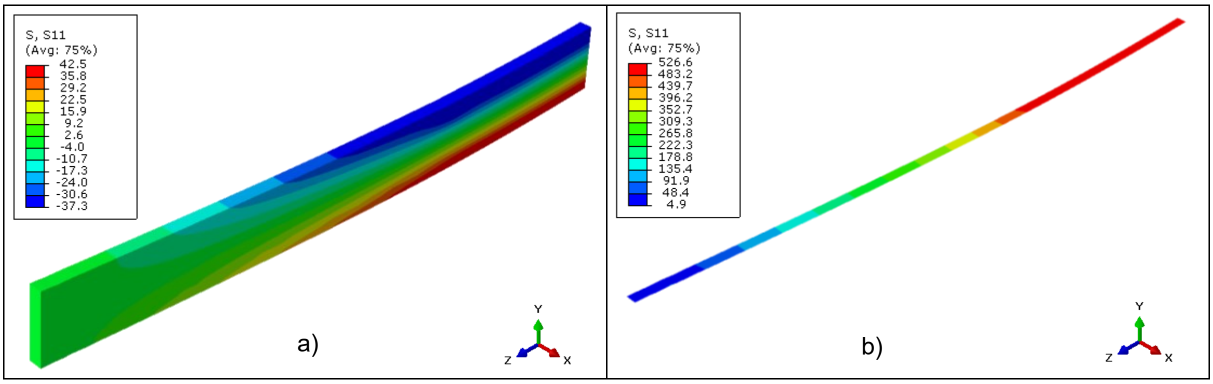

Fig. 9. Tensile stress σ_{11} (MPa) atthe moment of local failure of the reinforced beam: a) in glulam; b) in CFRP plate

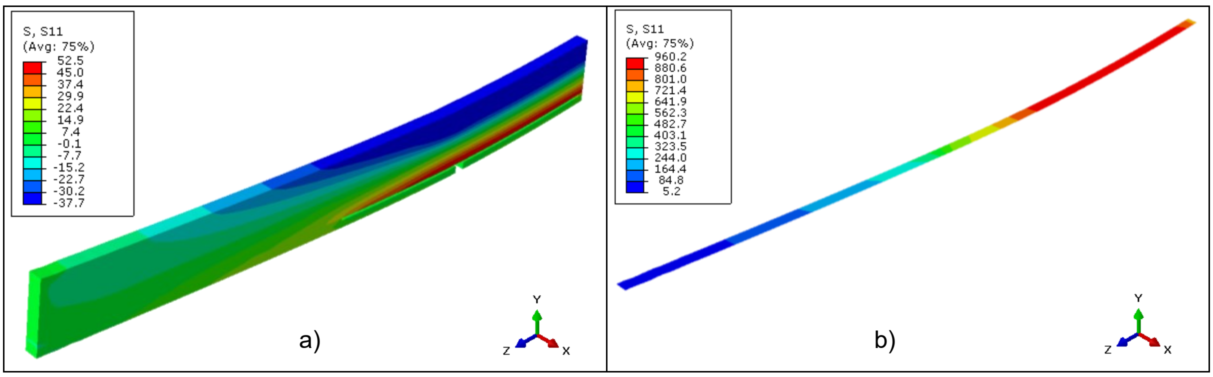

Fig. 10. Tensile stress σ_{11} (MPa) at the moment of global failure of the reinforced beam: a) in glulam; b) in CFRP plate

The results of experimental tests and numerical modelling in regard to ultimate load capacity, mid-span deflection at failure, and elastic bending stiffness, are summarized in Table 3. The effect of reinforcement on the ultimate load-carrying capacity, stiffness and deformability is clearly demonstrated. The last column compares the model's results with the average experimental results.

Table 3. Experimental and numerical results

Test series	Exp.	FEM	FEM/Exp. (%)
Maximum load (kN)			
Series A	37.9 (CV = 12.1 %)	39.0	2.9
Series F	46.4 (CV = 9.3 %)	47.6	2.7
Maximum mid-span deflection (mm)			
Series A	59.9 (CV = 10.0 %)	61.7	3.0
Series F	95.3 (CV = 25.2 %)	113.9	19.5
Bending stiffness *EI* (× 10^{11} Nmm^2)			
Series A	6.46 (CV = 7.7 %)	6.53	1.1
Series F	7.28 (CV = 6.2 %)	7.12	–2.2
CV – Coefficient of variation			

Numerical and experimental values of load-carrying capacity are very close with a difference of approximately 3% for both unreinforced and reinforced beams. In both cases, the predicted value of the maximum load was higher than the experimental value. It was anticipated that the results would differ even more when knots and other timber defects were taken into account.

The FE model predicted stiffness values agree well with those experimentally determined, with differences of about 2%. This small deviation proves the uniform quality of the laminations. Given that agreement is strong, it is confirmed that the assumption of perfect adhesion between the CFRP and timber is valid.

The mid-span deflection values show satisfactory compatibility for unreinforced beams. However, the numerical and experimental values of the mid-span deflection at failure show a noticeable difference of about 20% for Series F. The cause of this deviation is variability in the experimentally recorded fracture patterns of the beams. If two reinforced beams, which did not have characteristic failure mechanisms in two stages, are omitted from the experimental analysis (premature tensile failure – Beam F2 and shear failure – Beam F3), the obtained numerical value of deflection is lower than the experimental one, with better agreement of results (difference of 4.0%).

Fig. 11 illustrates the comparisons of experimental and numerical strain profiles at mid-span for different load levels.Strain distribution in mid-span across the height was linear until failure in the case of unreinforced beams. Tensile and compressive strains were almost identical at different load levels. The position of the neutral axis remained unchanged as the load increased, which proved there was no plasticization in the compression zone.

For the reinforced beams linear strain distribution across the height was observed in the elastic region. Neutral axis moved towards tension zone due to contribution of the CFRP plate. After failure of bottom lamination, neutral axis shifted upwards. No significant variation of neutral axis position was recorded as the applied load increased and plasticization in compression zone occurred. A non-linear strain distribution prior to global failure was noticed. In addition to improvement in tension strains, strain results demonstrated that timber compressive properties were better utilized when CFRP reinforcement was included in the tension zone.

Good agreement of the results is achieved from the simulated strain profiles for both sets of beams. The difference that exists between numerical predictions and experimental values is a result of an average timber modulus of elasticity being used for each lamination, when actually each lamination is inhomogeneous and material properties of timber vary throughout. Also, the reason for deviations in the nonlinear region can be explained by the assumption in the numerical analysis that plane sections remain plane after plastic deformation.

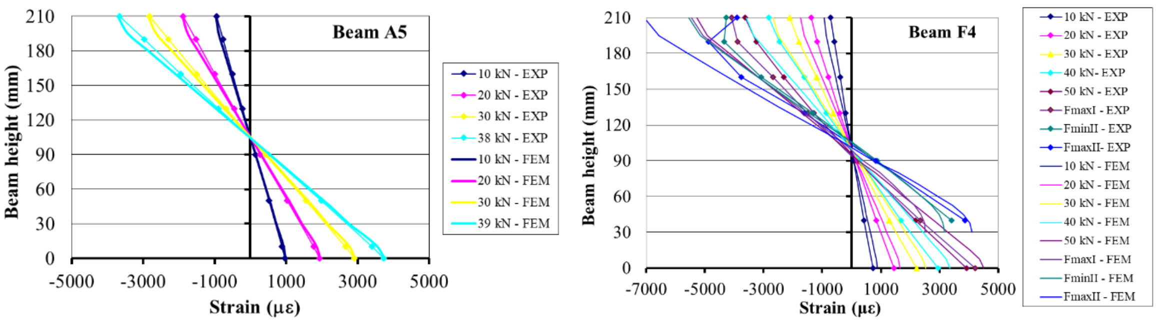

Fig. 11. Strain profiles at different load levels for unreinforced (Series A) and reinforced (Series F) beams

5 Conclusions

The effectiveness of FRP reinforcement of timber members has been proven through various studies.In order to better understand mechanical performance of CFRP plate reinforced glulam beams, a nonlinear finite element model was developed. Finite element modelling approach implemented in this paper was based on elasto-plastic and orthotropic characteristics of timber, Hill's plasticity criterion and progressive damage model to account for softening behaviour of timber in tension. Numerical predictions confirmed previousexperimental research.

Proposed FE models simulated experimentally obtained load-deflection curves and failure modes for both unreinforced and reinforced glulam beams. Numerical model demonstrated linear load-deflection behaviour and brittle tensile failure in bottom laminations of unreinforced beams. Predicted model for reinforced beams replicated failure in two stages:local failure of timber lamination below the reinforcement and global failure of the beam above the reinforcement, with significant nonlinear load-deflection behaviour. The progressive damage modelling has the ability to predict nonlinear response of reinforced beams accurately.

Good agreement between numerical and experimental data was found for bending stiffness, ultimate load-carrying capacity and mid-span deflection at failure. Numerical results demonstrated that adding the CFRP plate in the tension zone of the section improved the ultimate load-carrying capacity, stiffness and ductility of glulam beams. Furthermore, the strain profile distributions predicted by the FE models agreed well with the experimental findings. The assumption of plane sections is acceptable for glulam beams reinforced with CFRP composites.

The proposed numerical approach proved to be helpful in analysing test results and improving comprehension of stress and deformation states in timber and reinforcement. The developed model is easily adjustable to different loading configurations, beam dimensions and material properties. Therefore, it is a valuable tool that can be used to optimise the design of timber beams reinforced with FRP plates, including determination of optimal reinforcement percentage and arrangement.

CRediT authorship contribution statement

Ivan Glišović: Conceptualization, Investigation, Formal analysis, Supervision, Writing – review & editing.

Marija Todorović: Conceptualization, Methodology, Software, Writing – original draft

Nađa Simović: Writing – review & editing, Software.

Marko Pavlović:Methodology, Software.

Declaration of competing interest

The authors declare that they have no known competing financial interests or personal relationships that could have appeared to influence the work reported in this paper.

Acknowledgement

This research was supported by the Science Fund of the Republic of Serbia, Serbian Science and Diaspora Collaboration Program: Knowledge Exchange Vouchers: Hybrid structures and connection of timber and FRP.

References

[1] J. Fiorelli, A.A. Dias, Glulam beams reinforced with FRP externally bonded: Theoretical and experimental evaluation. Materials and Structures 44(8) (2011) 1431-1440. https://doi.org/10.1617/s11527-011-9708-y.

[2] G.M. Raftery, A.M. Harte, Low-grade glued laminated timber reinforced with FRP plate. Composites: Part B 42(4) (2011) 724-735. http://dx.doi.org/10.1016/j.compositesb.2011.01.029.

[3] Y.J. Kim, M. Hossain, K.A. Harries, CFRP strengthening of timber beams recovered from a 32 year old Quonset: Element and system level tests. Engineering Structures57 (2013) 213-221.https://doi.org/10.1016/j.engstruct.2013.09.028.

[4] G.M. Raftery, C. Whelan, Low-grade glued laminated timber beams reinforced using improved arrangements of bonded-in GFRP rods. Construction and Building Materials52 (2014) 209-220.
https://doi.org/10.1016/j.conbuildmat.2013.11.044.

[5] A. D'Ambrisi, F. Focacci, R. Luciano, Experimental investigation on flexural behaviorof timber beams repaired with CFRP plates. Composite Structures 108 (2014) 720-728.
https://doi.org/10.1016/j.compstruct.2013.10.005

[6] I. Glišović, B. Stevanović, M. Todorović, Flexural reinforcement of glulam beams with CFRP plates. Materials and Structures 49(7) (2016) 2841-2855. https://doi.org/10.1617/s11527-015-0690-7

[7] H. Yang, W. Lin, W. Lu, S. Zhu, O.Geng, Flexural behaviour of FRP and steel reinforced glulam beams: Experimental and theoretical evaluation. Construction and Building Materials 106 (2016) 550-563. https://doi.org/10.1016/j.conbuildmat.2015.12.135

[8] B. Kasal, L. Yan, Fibre-reinforced polymers as reinforcement for timber structural elements,in: J. Branco, P. Dietsch, T. Tannert (Eds.), Reinforcement of timber elements in existing structures, State-of-the-Art Report of the RILEM TC 245-RTE, Springer, 2021, pp. 51–78.

[9] M. Todorović, I. Glišović, B. Stevanović, Experimental investigation of end-notched glulam beams reinforced with GFRP bars. European Journal of Wood and Wood Products 80(5) (2022) 1071-1085.
https://doi.org/10.1007/s00107-022-01822-6

[10] T.P. Nowak, J. Jasienko, D. Czepizak, Experimental tests and numerical analysis of historic bent timber elements reinforced with CFRP strips. Construction and Building Materials 40 (2013) 197-206.https://doi.org/10.1016/j.conbuildmat.2012.09.106

[11] M. Szczecina, Study of Complexity of Numerical Models of a Strengthened Timber Beam. Materials 16 (2023) 3466.https://doi.org/10.3390/ma16093466

[12] G.M. Raftery, A.M. Harte, Nonlinear numerical modelling of FRP reinforced glued laminated timber. Composites: Part B 52 (2013) 40-50. https://doi.org/10.1016/j.compositesb.2013.03.038

[13] M. Khelifa, S. Auchet, P.J. Meausoone, A. Celzard A, Finite element analysis of flexural strengthening of timber beams with carbon fibre reinforced polymers. Engineering Structures 101 (2015) 364-375. https://doi.org/10.1016/j.engstruct.2015.07.046

[14] rach, H. Muayad, R. Majid Movahedi, Reliability-based numerical analysis of glulam beams reinforced with CFRP plate. Scientific Reports 12 (2022) 13587.https://doi.org/10.1038/s41598-022-17751-6

[15] EN 338: Structural timber - Strength classes, European Committee for Standardization, Brussels, Belgium, 2009.

[16] Sika CarboDur plates: Pultruded carbon fibre plates for structural strengthening, 2015. Product Data Sheet, Sika AG, 2015.

[17] EN 408: Timber structures - Structural timber and glued laminated timber - Determination of some physical and mechanical properties, European Committee for Standardization, Brussels, Belgium, 2010.

[18] Abaqus/CAE. User's Guide, Version 2017; Dassault Systems Simulia Corp: Johnston, RI, USA, 2016.

[19] R.D.S.G. Campilho, M.F.S.F. de Moura, A.M.J.P. Berreto, J.J.L. Morais, J.J.M.S. Domingues, Fracture behaviour of damaged wood beams repaired with an adhesively-bonded composite patch. Composites: Part A 40 (2009) 852-859. https://doi.org/10.1016/j.compositesa.2009.04.007

[20] J. Bodig, B.A. Jayne, Mechanics of wood and wood composites. Van Nostrand Reinhold Company, New York, 1982.

[21] B. Harris, Engineering composite materials. The Institute of Materials, London, 1999.

[22] M. Wang, X. Song, X. Gu, Three-dimensional combined elastic-plastic and damage model for nonlinear analysis of wood. Journal of Structural Engineering 144(8) (2018) 04018103.https://doi.org/10.1061/(ASCE)ST.1943-541X.0002098

[23] C. Sandhaas, J.W.G. van de Kuilen, Material model for wood. HERON 58(2/3), 2013.

Građevinski materijali i konstrukcije
Building Materials and Structures
journal homepage: www.dimk.rs

https://doi.org/10.5937/GRMK2500004R UDK: 666.97/.98.01

Original scientific paper

Impact of the water-curing time on the carbonation initiation period of high-volume limestone powder concrete

Andrija Radović[1)], Vedran Carević[2)], Snežana Marinković[*2)]

[1)] *University of Priština in Kosovska Mitrovica, Faculty of Technical Sciences, Knjaza Miloša 7, 38220, Kosovska Mitrovica, Serbia*
[2)] *University of Belgrade, Faculty of Civil Engineering, Bulevar kralja Aleksandra 73, 11000, Belgrade, Serbia*

Article history

Received: 30 April 2025
Received in revised form: 26 May 2025
Accepted: 27 May 2025
Available online: 13 June 2025

Keywords

high-volume limestone powder concrete,
carbonation resistance,
curing time,
Model Code 2020,
execution transfer parameter

ABSTRACT

The high-volume limestone powder concrete (HVLPC) is one of the potential CO_2 mitigation strategies within ready-mixed concrete sector. As with other low-clinker concretes, its durability related properties, carbonation resistance especially, could present a problem in the structural applications. This work deals with the influence of the water-curing time on the carbonation initiation period of HVLPC. An experimental campaign was designed which included various curing times, from 1 day to 28 days. Beside the reference mix (ordinary Portland cement concrete - OPC), HVLPC mixes with three different percentages of limestone powder (LP) in the powder phase (47%, 58% and 65%), and with two different LP particle size distributions within each group, were designed to have similar compressive strength. All mixes were tested under accelerated and natural carbonation conditions. Test results showed significant impact of the curing time on the HVLPC carbonation resistance, but different from OPC. The Model Code 2020 prediction model was tested against test results and it was found that it largely overestimated the impact of curing duration for short curing times (1 and 3 days), while underestimated this impact for 14 and 28 days of curing. New expression for the execution transfer parameter kc was proposed based on the own experimental results.

1 Introduction

In a pure mass-flow sense, concrete is by far the largest human-made product. Some research showed that human made mass, with concrete and aggregates making its large majority already exceeded all living biomass on Earth [1]. According to Global Cement and Concrete Association GCCA [2], 14 billion m^3 of concrete was produced in 2020. Global average of CO_2 emissions per tonne of cement varied between 0.6-0.7 tonnes in 2020 depending on the source, including energy related emissions [3-4]. If global yearly cement production is about 4.1 Gt, cement production emits approximately 2.7 Gt of CO_2 per year. This made about 7% of total CO_2 anthropogenic emissions in 2022, which were about 40 Gt according to [5].

About two-third of CO_2 emissions [6] in cement production originates from the decomposition of limestone (calcination) and the rest is associated with energy use. Because of that, cement industry is considered one of the most difficult to decarbonize as decarbonisation of the energy supply will not eliminate the unavoidable CO_2 emissions from calcination [7].

There are multiple ways of reducing CO_2 emissions from cement and concrete production. Savings in cement content, including the clinker substitution with so-called supplementary cementitious materials (SCM), is one of them. However, it is expected that global availability of the most widely used SCMs, fly ash (FA) and blast furnace slag (BFS), will decrease in near and medium term. FA comes from coal power plants and BFS from the steel industry's blast furnaces and these industries are also transitioning [8]. Therefore, other suitable materials must be looked for. Limestone is currently also used as SCM but in small quantities. Since it is abundantly available all over the world, the attempt was made in previous research to increase the participation of the limestone powder in the binder content and therefore to reduce CO_2 emissions from cement and concrete production.

Concrete with high amount of the limestone powder (over 35% in the powder phase) is called high-volume limestone powder concrete – HVLPC. Previous research showed that it was possible to achieve the HVLPC mechanical properties required for the structural concrete, if optimisation of the paste composition, improved particle packing and lowering the water content were applied [9-12]. However, the carbonation resistance remained significantly lower compared with reference clinker-based concrete due to lower alkalinity and higher porosity of HVLPC [13-17].

[*] Corresponding author:
E-mail address: sneska@grf.bg.ac.rs

Prediction models developed for carbonation initiation period of clinker-based concrete are not directly applicable to HVLPC, as shown by [17, 18].

Radović et al. [17] proposed modification of the Model Code 2010 [19] prediction model for the carbonation depth calculation in the initiation period. The proposed relationship between inverse effective carbonation resistance under natural and accelerated conditions was based on the statistical analysis of experimental results, own and available in literature. However, the authors assumed that curing impact (k_c) proposed in the Model Code 2010 equation was valid for the HVLPC as well. This assumption has to be experimentally verified since curing type and time can differently affect the carbonation initiation period in HVLPC [20]. The problem was rarely investigated in the previous research and the only experimental results found in literature were those reported in [21]. However, the authors tested concretes with up to 30% cement replacement with limestone powder (LP), which cannot be considered as HVLPC.

The objective of this work was to experimentally determine the impact of the curing time on the HVLPC carbonation resistance, and to propose the empirical equation for the execution transfer parameter k_c within the Model Code 2020 (MC 2020) [22] carbonation initiation model. For that reason, an experimental campaign was designed which included various water-curing times, from 1 day to 28 days. Beside the reference mix (ordinary Portland cement concrete - OPC), HVLPC mixes with three different percentages of LP in the powder phase (47%, 58% and 65%), and with two different LP particle size distributions within each group, were designed to have similar compressive strength. All mixes were tested under accelerated and natural (420 days, indoor) carbonation conditions.

2 Experimental procedures

2.1 Component materials and concrete mixture proportions

For this experimental campaign, Ordinary Portland cement CEM I 42.5R [23] with corresponding mean particle size of d_{50} = 11.1 μm (Figure 1) was used. The density of cement was approximately 3100 kg/m^3. The effect of limestone fineness was evaluated using two high-purity LPs, with the same chemical composition (98% $CaCO_3$ content, meeting the EN 197-1 [23] requirements), but different particle size distributions. Determination of particle size distribution was done by laser diffraction method. Limestone powder L_{12} had a particle size distribution (d_{50} = 11.7 μm) similar to OPC, while limestone powder L_3 contained much finer particles (d_{50} = 2.9 μm), Figure 1. The densities of L_3 and L_{12} were about 2720 kg/m^3 and 2690 kg/m^3, respectively.

Locally available river aggregate, divided into three fractions I (0-4 mm), II (4-8 mm) and III (8-16 mm) was applied. The participation of each fraction in the total aggregate quantity (Table 1) was 52%, 21%, and 27% respectively. The workability of fresh concrete was controlled by adjusting the dosage of a polycarboxylate-based superplasticizer.

The target workability class for all mixtures was S4 or S5, with a required slump of ≥ 200 mm, as specified in EN 206-1 [24]. To achieve a meaningful comparison of the results, the target compressive strength was set at $f_{cm,cube}$ = 50±5 MPa, determined using 100 mm cube specimens. This strength range aligns with widely used concrete classes C25/30 and C30/37 according to Eurocode 2 [25]. By selecting this compressive strength, the study ensures that the tested mixtures reflect typical structural concrete applications, allowing for a realistic evaluation of performance. The chosen strength classes also facilitate direct comparisons with existing standards recommendations for commonly used concrete mixtures in construction practice.

Mixtures proportions were determined by the absolute volume method. In the reference mixture, the cement content was 334 kg/m³, and it was partially replaced by 30%, 45%, and 55% using each of L_3 and L_{12} limestone powder respectively. To ensure that the compressive strength remained within the desired target range, it was necessary to reduce the water-to-cement (w/c) ratio in mixtures incorporating limestone powder. This reduction resulted in a lower volume of cement paste, requiring an adjustment in the mixture composition. Consequently, a greater amount of limestone powder was added compared to the quantity of cement replaced, in order to compensate for the volumetric changes and maintain the overall performance of the concrete. The mixture proportions of the tested concretes are presented in Table 1. The mixture designation consists of the type of limestone powder (L_3 or L_{12}) and its mass percentage in the total powder phase (cement + limestone) of the concrete, which were 47%, 58%, and 65%.

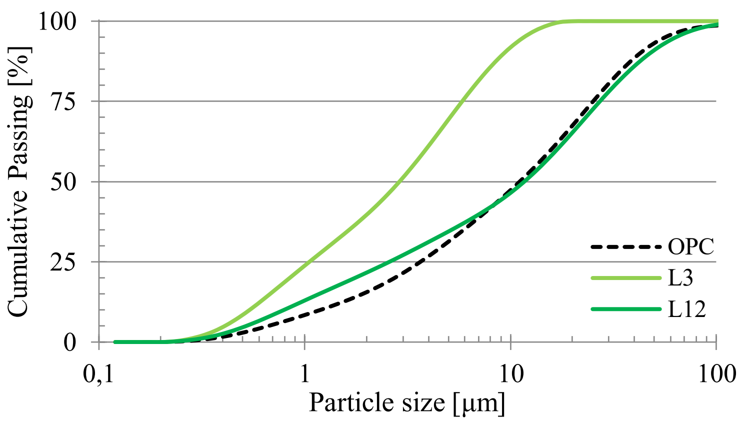

Figure 1. Particle size distribution of cement and limestone powders

Table 1. Proportions of concrete mixtures

Concrete mix	m_c [kg/m^3]	m_{LS} [kg/m^3]	m_w [kg/m^3]	w/c [–]	Aggregate [kg/m^3]	SP [kg/m^3]
OPC	334	0	171	0.51	1874	3.30
L_3-47	230	200	143	0.62	1847	6.45
L_{12}-47	230	200	143	0.62	1846	6.45
L_3-58	182	252	127	0.70	1868	8.60
L_{12}-58	182	252	127	0.70	1866	8.60
L_3-65	153	285	114	0.75	1883	8.60
L_{12}-65	153	285	114	0.75	1881	8.60

2.2 Preparation, casting, curing, and testing of concrete specimens

The mixing process for each concrete mixture lasted a total of five minutes. After verification of the workability with a standard slump test [26], the concrete was cast into moulds and compacted immediately after placing. The specimens were then covered with a plastic sheet to prevent moisture loss and stored in the laboratory environment. After 24 hours, the specimens were demoulded and subjected to five different curing conditions for a period of 28 days. The curing conditions are identified by numbers corresponding to the duration of standard curing (1, 3, 7, 14, and 28 days), as defined in [26]. A detailed description of these curing conditions is provided in Table 2.

Compressive strength at 28 days was tested on 100 mm cubic samples, following the EN 12390-3 [27], using three cubes for each mixture and each curing condition.

The carbonation resistance was assessed using 120×120×360 mm prismatic specimens, with two prisms prepared for each mixture. After completing the 28-day initial curing (as described in Table 2), the specimens underwent an additional 14-day conditioning in a climate chamber at 20±2°C and 65±5% relative humidity, to ensure uniform moisture distribution before carbonation exposure. Following this period, the prisms were halved, with one half exposed to accelerated carbonation and the other half used for a natural carbonation test. The accelerated carbonation test was conducted in a carbonation chamber under controlled conditions of 2% CO_2, 20±2°C, and 65±5% relative humidity for 28 days. In contrast, specimens designated for natural carbonation were stored under laboratory conditions (Figure 2) for 420 days to simulate long-term environmental exposure. The mean values and standard deviations of the laboratory environment parameters (relative humidity, temperature, and CO_2 concentration) are detailed in Table 3. The final carbonation depth, for both accelerated and natural carbonation, was determined as the average of eight measurements taken on each side of each prism, in accordance with EN 14630 [28].

Table 2. Curing conditions

Curing period	Curing (1d)	Curing (3d)	Curing (7d)	Curing (14d)	Curing (28d)
1 day	Mould	Mould	Mould	Mould	Mould
1-3 days	Air*	Water	Water	Water	Water
3-7 days	Air	Air	Water	Water	Water
7-14 days	Air	Air	Air	Water	Water
14-28 days	Air	Air	Air	Air	Water

*Air – laboratory-controlled environment (20°C, 65% RH); Water (20°C)

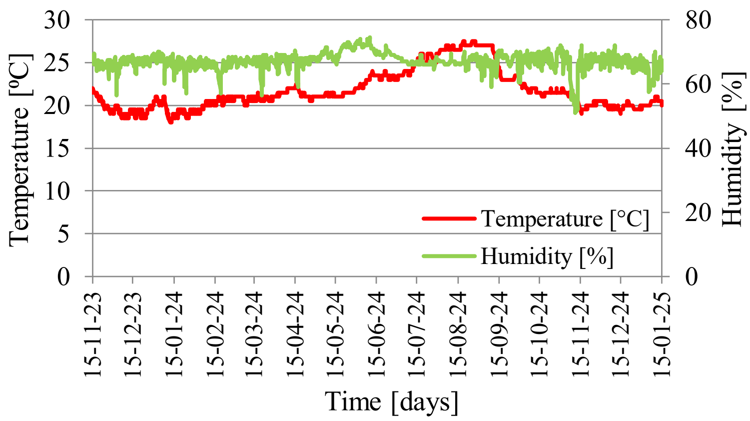

Figure 2. Natural environmental conditions during testing

Table 3. Mean values and standard deviations of environmental conditions

	Temperature [°C]	Relative humidity [%]	CO_2 [ppm]
Mean	21.8	67.1	440
St. deviation	2.3	2.8	70.5

3 Results and discussion

The compressive strengths measured at 28 days for cube samples ($f_{cm,cube}$) and calculated for cylinder samples ($f_{cm,cyl}$), for concrete mixes cured under various conditions, are presented in Table 4.

Table 4. Measured properties of tested concrete mixtures

Mixtures	Curing period [days]	$f_{cm,cube}$ [MPa]	$f_{cm,cyl}$ [MPa]
OPC	1	49.8	37.4
	3	52.4	39.3
	7	52.9	39.7
	14	51.1	38.3
	28	50.1	37.6
L_3-47	1	52.3	39.2
	3	51.3	38.5
	7	55.4	41.6
	14	55.9	41.9
	28	50.2	37.7
L_{12}-47	1	52.9	39.7
	3	53.6	40.2
	7	55.8	41.9
	14	55.7	41.8
	28	50.2	37.7
L_3-58	1	50.7	38.0
	3	54.1	40.6
	7	54.6	41.0
	14	53.4	40.1
	28	44	33.0
L_{12}-58	1	48.3	36.2
	3	50.3	37.7
	7	54.3	40.7
	14	52.4	39.3
	28	47.8	35.9
L_3-65	1	56.1	42.1
	3	57.4	43.1
	7	57.9	43.4
	14	61.6	46.2
	28	51.8	38.9
L_{12}-65	1	46.0	34.5
	3	47.5	35.6
	7	51.2	38.4
	14	49.4	37.1
	28	45.4	34.1

The results showed that there was practically no difference in compressive strength of HVLPC mixes with different fineness of LP (the differences were within 0.6%) for L-47 and L-58 concretes. In mixes with the highest LP content (L-65), limestone powder with higher fineness provided higher compressive strength. The increase of compressive strength was 20% (mixes with L_3 compared to mixes with L_{12} powder which is similar to cement). Except for the L_{12}-65 mix, the compressive strengths of the HVLPC mixes were similar to those of the reference OPC concrete. For all samples cured in water for 28 days, the measured compressive strengths varied between 45.4 and 51.8 MPa, aligning with the initial hypothesis of producing concrete mixes with consistent strength of 50±5 MPa. The only concrete that had strength lower than 45 MPa was L_3-58, whose strength was 44 MPa for samples cured for 28 days in water. However, all samples of this concrete cured for less than 28 days had strength greater than 50 MPa.

The 7 days curing period had a beneficial impact on the achieved compressive strength values, with longer curing period leading to lower compressive strengths. Concrete mixes cured in water for 28 days exhibited the lowest compressive strength compared to all other curing regimes. This outcome may be attributed to the increased amount of water absorbed by the concrete, which remained within the material at the time of testing under compressive load. The retained water, when subjected to external pressure, generates internal stresses and water vapor pressure, which ultimately reduces the fracture toughness of the concrete. Similar conclusions were reached in the study [29]. It is assumed that complete drying of samples cured in water for 28 days would result in greater compressive strength compared to alternative curing methods. As for curing time of 14 days, all concrete mixes showed compressive strengths approximately equal to those of concrete mixes cured for 7 days in water, with the exception of the L_3-65 mix.

As observed, curing had a more pronounced influence on the development of compressive strength in the HVLPC than in the OPC concrete. Among the HVLPC mixes, the curing regime's contribution to strength development appeared independent of the fineness of the LP. Additionally, variations in curing conditions did not significantly affect the rate of strength gain of the tested concretes.

Measured carbonation depths under accelerated (ACC) conditions after 28 days of exposure and natural (NAC) conditions after 420 days of exposure, along with the relationships between carbonation depth and water-curing period for all concrete mixtures, are shown in Figures 3 and 4. It can be seen that with increasing the water-curing period, the carbonation depth decreases. However, the effect of curing was smallest with the reference OPC concrete (17%). As for HVLPC mixes, the impact of water-curing duration increased with the LP content increase in both accelerated and natural conditions. The trend was similar for both types of LP. What however is interesting is that the mixes with 47%

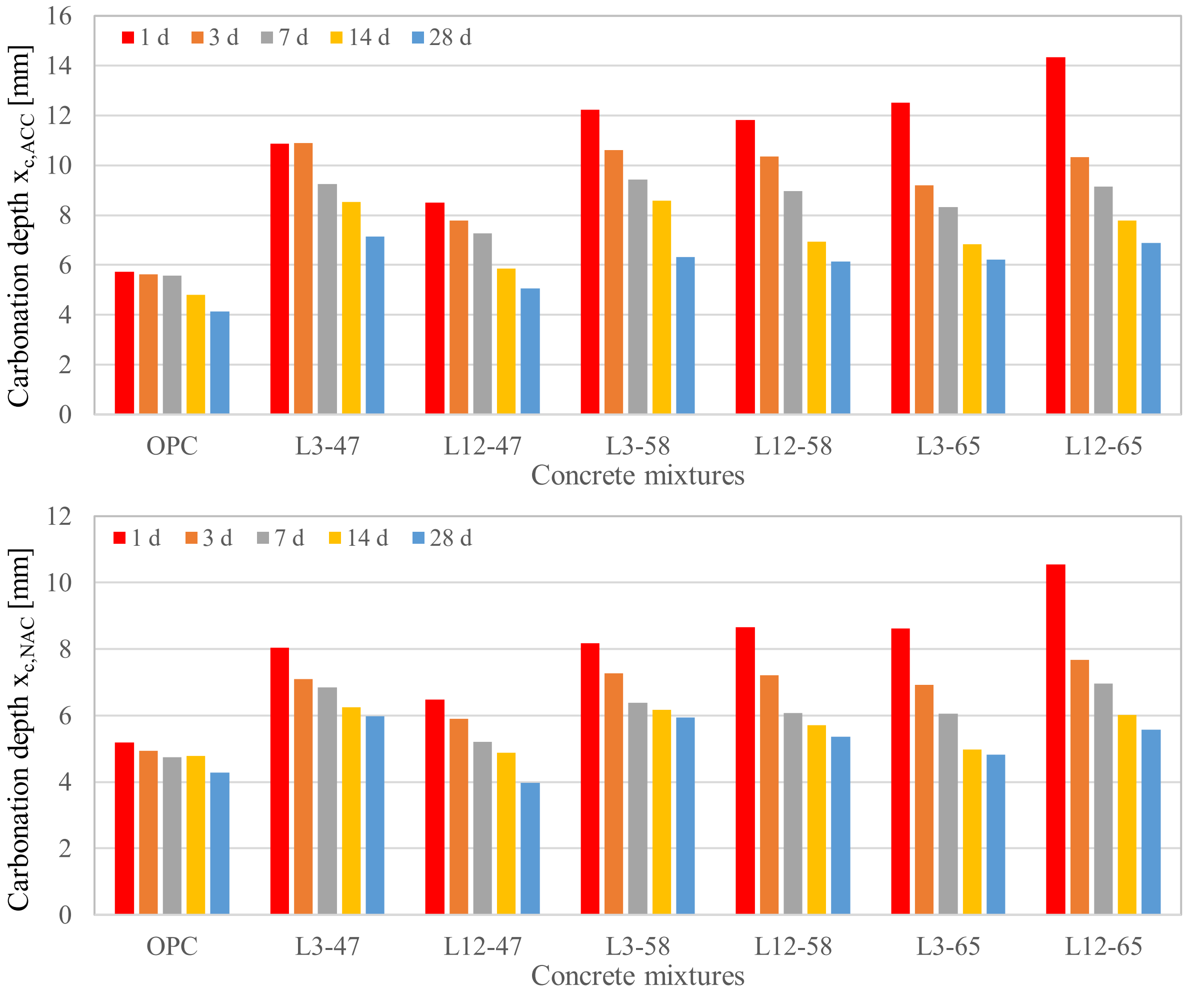

Figure 3. Measured carbonation depths under accelerated (ACC) and natural (NAC) conditions for different curing periods

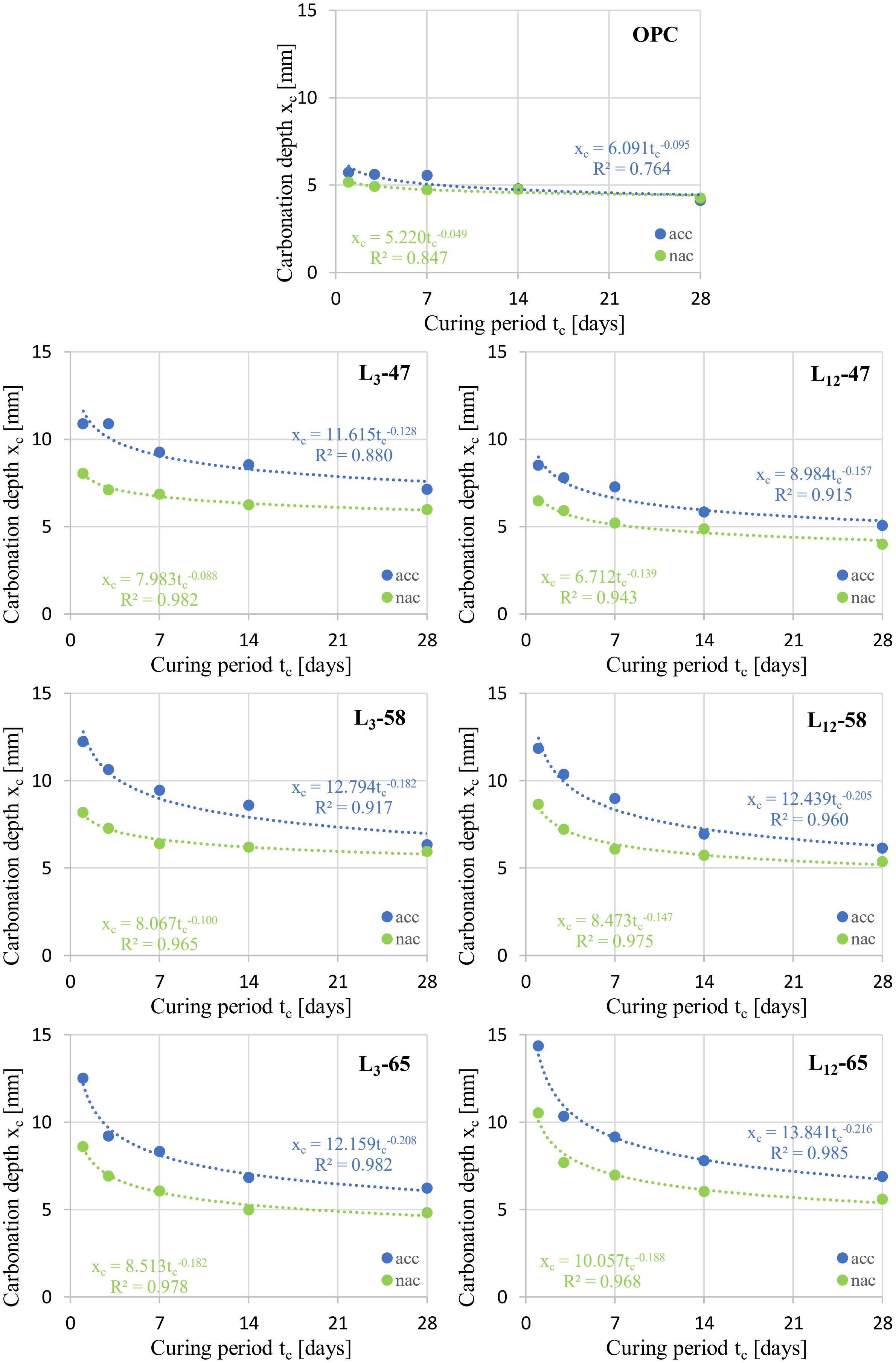

Figure 4. The relationship between the carbonation depth and water-curing period

and 58% of finer LP had generally higher carbonation depths compared with those mixes made with coarser LP for all curing periods. Only the L-65 mix with finer LP had lower carbonation depths under natural conditions (the carbonation depth of L_3-65 was 13%-19% lower compared to L_{12}-65, depending on the curing duration). This is in contrast to the results published in [29], where concrete mixes with finer LP had a lower carbonation depth.

In all cases, the HVLPC mixtures had lower carbonation resistance compared to the reference OPC concrete, although the compressive strength was generally similar or higher. The only mixture that had higher resistance was L_{12}-47, which had a 7% lower carbonation depth. Although the proposed mix design method – characterized by low water content and high plasticizer dosage – successfully maintained compressive strength, the issue of low alkaline reserve persisted, resulting in reduced carbonation resistance. Nevertheless, the test results demonstrated that it is feasible to design concrete mixes that meet both high workability and strength requirements for commonly used strength classes, using as little as 153 kg/m^3 of cement. However, HVLPC mixes had up to 40% greater carbonation depth in natural conditions compared to OPC, for standardly cured samples of 28 days. Generally, the measured carbonation depths after 420 days correspond to the expected values that can be found in the literature for these types of concrete [18].

In order to examine the influence of water-curing period on the HVLPC carbonation resistance, the MC 2020 [22] carbonation depth prediction model was applied. This model includes execution transfer parameter (k_c) that takes into account concrete curing period:

$$k_c = \left(\frac{t_c}{7}\right)^{b_c} \tag{1}$$

where t_c is the period of moist curing (days), while b_c is exponent of regression with mean value equal to -0.567 and standard deviation equal to 0.024 (normal distribution). However, this exponent was calibrated on the ordinary and blended cement based concretes [30]. For concretes with up to 30% cement replacement with LP, this relationship was tested by Lollini & Redaelli [21], suggesting that this exponent should be -0.10. This relationship was evaluated as well for concretes tested in this research, i.e. concretes with more than about 50% in the powder phase.

In order to evaluate the relationship (1) for the tested HVLPC mixes, it was necessary to determine the coefficient k_c experimentally. This was done based on the measured values of natural carbonation depths of concretes cured for different curing periods $k_{c,t}$:

$$\frac{x_{c,t}}{x_{c,ref}} = \sqrt{\frac{k_{c,t}}{k_{c,ref}}} = \sqrt{k_{c,t}} \tag{2}$$

where

$x_{c,t}$ carbonation depth of concrete water-cured for time t

$x_{c,ref}$ carbonation depth of concrete water-cured for 7 days

$k_{c,t}$ execution transfer parameter for concrete water-cured for time t

$k_{c,ref}$ execution transfer parameter for concrete water-cured for 7 days, $k_{c,ref} = k_{c,7} = 1$

Using the previously defined relationship (2), the coefficients k_c for OPC and HVLPC mixes were calculated based on the measured carbonation depths under natural conditions. Figure 5 shows the relationship between the execution transfer parameter (k_c) and duration of water-curing. In addition to the experimental results, the figure shows the MC 2020 relationship and Lollini & Redaelli [21] proposal as well.

The relationship between k_c and t_c in the form:

$$k_c = \left(\frac{t_c}{7}\right)^{-0.281} \tag{3}$$

fits well the test results for all HVLPC mixes, regardless of the content and fineness of LP ($R^2 = 0.88$). The MC 2020 expression for k_c largely overestimates the impact of water-curing duration for short curing times (1 and 3 days), while underestimates this impact for 14 and 28 days of curing. The

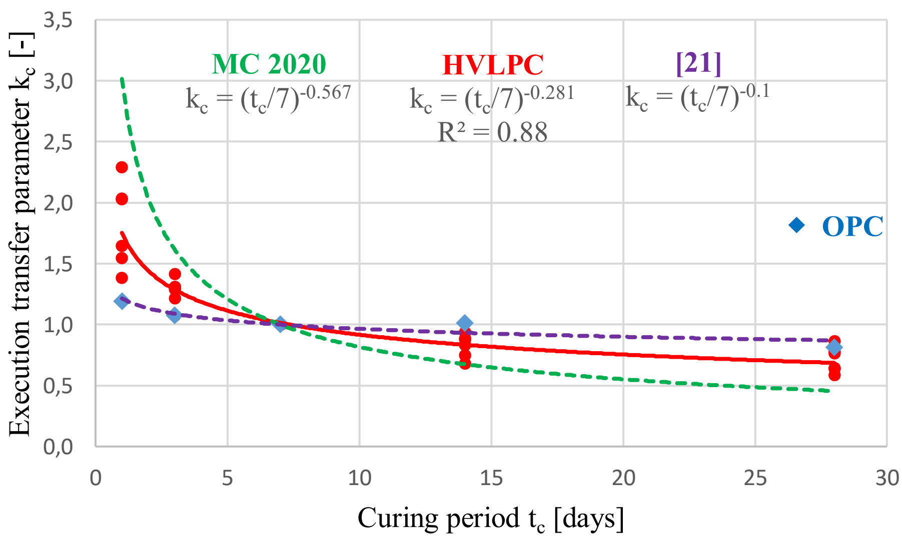

Figure 5. Relationship between execution transfer parameter (k_c) and water-curing period (t_c)

MC 2020 prediction behaves even worse for the tested OPC mix. This is probably the consequence of the calibration of this parameter on the mixes made with both OPC and commercial blended cements, which gave a large scatter of results, especially for curing periods of 1 and 3 days [31]. On the other hand, Lollini & Redaelli [21] proposal made originally for mixes with up to 30% of the LP fits well the OPC mix test results, suggesting that such mixes behaved similarly to OPC concrete. Having in mind that only one OPC mix was tested in this research, this is only a remark, not the conclusion.

4 Conclusions

The results of the experimental testing of the compressive strength and carbonation depth (under accelerated and natural conditions) of reference OPC mix and six different HVLPC mixes were presented. All mixes were water-cured for 1, 3, 7, 14, and 28 days, and for each curing period compressive strength and carbonation depth were determined. Following conclusions were drawn:

- the compressive strength at 28 days of all mixes varied between 44 MPa and 51.8 MPa (i.e. between 33 and 39 on cylindrical specimens);
- except for the L_{12}-65 mix, the compressive strengths of the HVLPC mixes were similar to those of the reference OPC concrete for all curing periods;
- among the HVLPC mixes, the impact of the curing regime on the strength development appeared independent of the fineness of the LP;
- with prolonging the water-curing period, the carbonation depths of all mixes decreased, i.e. carbonation resistance increased;
- impact of the water-curing period on the carbonation resistance is much more pronounced for the HVLPC mixes than for the reference OPC mix;
- impact of the water-curing duration slightly increased with the LP content increase in both accelerated and natural conditions regardless of the LP fineness;
- the MC 2020 expression for the execution transfer parameter k_c is hardly applicable to HVLPC for all tested LP contents and fineness.

The new expression for the execution transfer parameter k_c, which describes the effect of the water-curing time on the HVLPC carbonation resistance, was proposed. The conclusions and the proposal are limited to experimental results obtained within this research.

CRediT authorship contribution statement

A. Radović: Data curation, Investigation, Formal analysis, Resources, Writing - original draft.

V. Carević: Data curation, Investigation, Methodology, Formal analysis, Writing - original draft.

S. Marinković: Conceptualization, Methodology, Supervision, Writing - review & editing.

Declaration of competing interest

The authors declare no conflict of interest.

Acknowledgments

This work was performed within the PhD thesis of Andrija Radović, student of the Doctoral Studies at the Faculty of Civil Engineering, University of Belgrade. We gratefully acknowledge the support of the laboratory staff at the Department of Materials and Structure.

References

[1] E. Elhacam, L. Ben-Uri, J. Grozovski, Y.M. Bar-On, R. Milo, Global human-made mass exceeds all living biomass, Nature 588 (7838) (2020), 442-444, https://doi.org/10.1038/s41586-020-3010-5

[2] GCCA. Concrete Future – The GCCA 2050 Cement and Concrete Industry Roadmap for Net Zero Concrete, 2021. Available at: https://gccassociation.org/concretefuture/

[3] Cembureau. Key Facts and Figures, 2024. Available at: https://cembureau.eu/about-our-industry/key-facts-figures/

[4] S. Boehm et al., State of Climate Action 2022, Bezos Earth Fund, Climate Action Tracker, Climate Analytics, Climate Works Foundation, New Climate Institute, the United Nations Climate Change High-Level Champions, and World Resources Institute, 2023. Available at: https://doi.org/10.46830/wrirpt.22.00028

[5] P. Friedlingstein et al., Global Carbon Budget 2023, Earth Syst. Sci. Data 15 (2023), 5301–5369, https://doi.org/10.5194/essd-15-5301-2023

[6] A. Favier, C. de Wolf, K. Scrivener, G. Habert, A sustainable future for the European cement and concrete industry, ETH Zürich, 2018. Available at: https://www.research-collection.ethz.ch/handle/20.500.11850/301843

[7] G. Habert, S.A.Miller, V.M. John et al., Environmental impacts and decarbonization strategies in the cement and concrete industries. Nature Reviews Earth & Environment 11 (2020), 559-573. https://doi.org/10.1038/s43017-020-0093-3

[8] UN Environment, K.L. Scrivener, V.M. John, E.M. Gartner, Eco-efficient cements: Potential economically viable solutions for a low-CO2 cement-based materials industry, Cement and Concrete Research 114 (2018), 2–26. https://doi.org/10.1016/j.cemconres.2018.03.015

[9] T. Proske, S. Hainer, M. Rezvani, C.A. Graubner, Eco-friendly concretes with reduced water and cement contents — Mix design principles and laboratory tests, Cement and Concrete Research 51 (2013), 38–46, http://dx.doi.org/10.1016/j.cemconres.2013.04.011

[10] J.J. Chen, A.K .H. Kwan, Y. Jiang, Adding limestone fines as cement paste replacement to reduce water permeability and sorptivity of concrete, Construction and Building Materials 56 (2014), 87–93, http://dx.doi.org/10.1016/j.conbuildmat.2014.01.066

[11] K. Robalo, E. Soldado, H. Costa, R. do Carmo, H. Alves, E. Júlio, Efficiency of cement content and of compactness on mechanical performance of low cement concrete designed with packing optimization, Construction and Building Materials 266 (2021), 121077, https://doi.org/10.1016/j.conbuildmat.2020.121077

[12] K. Tešić, S. Marinković, A. Savić, Influence of cement replacement with limestone filler on the properties of concrete, Gradjevinski materijali i konstrukcije (Building Materials and Structures) 64 (2021), 165-170, http://dx.doi.org/10.5937/GRMK2103165T

[13] S. Palm, T. Proske, M. Rezvani, S. Hainer, C. Müller, C.A. Graubner, Cements with a high limestone content – Mechanical properties, durability and ecological characteristics of the concrete, Construction and Building Materials 119 (2016), 308–318, http://dx.doi.org/10.1016/j.conbuildmat.2016.05.009

[14] S. Steiner, T. Proske, F. Winnefeld, B. Lothenbach, Effect of limestone fillers on CO_2 and water vapour diffusion in carbonated concrete, Cement 8 (2022), 100027, https://doi.org/10.1016/j.cement.2022.100027
[15] K. Robalo, E. Soldado, H. Costa, L. Carvalho, R. do Carmo, E. Júlio, Durability and Time-Dependent Properties of Low-Cement Concrete, Materials 13 (2020), 3583, https://dx.doi.org/10.3390/ma13163583
[16] M. Marinković, A. Radović, V. Carević, Carbonation of limestone powder concrete: state-of-the-art overview, Gradjevinski materijali i konstrukcije (Building Materials and Structures) 66 (2023), 2300005M, https://doi.org/10.5937/GRMK2300005M
[17] A. Radović, V. Carević, S. Marinković, J. Plavšić, K. Tešić, Prediction model for calculation of the limestone powder concrete carbonation depth, Journal of Building Engineering 86 (2024), 108776. https://doi.org/10.1016/j.jobe.2024.108776
[18] V. Carević, S. Marinković, J. Plavšić, A. Radović, Service life design of concrete structures made of high-volume limestone powder concrete - case of the carbonation induced corrosion, Buildings 13 (2023), 3112. https://doi.org/10.3390/buildings13123112
[19] fib, Model code 2010 final draft, vol. 2. fib Bulletin, N. 66, Lausanne, 2012.
[20] Z. Zhang, Q. Wang, H. Chen, Properties of high-volume limestone powder concrete under standard curing and steam-curing conditions, Powder Technology 301 (2016), 16–25, http://dx.doi.org/10.1016/j.powtec.2016.05.054
[21] F. Lollini, E. Redaelli, Carbonation of blended cement concretes after 12 years of natural exposure, Construction and Building Materials 276 (2021), 122122, https://doi.org/10.1016/j.conbuildmat.2020.122122
[22] fib, Model code for concrete structures 2020 final draft, International federation for Structural concrete, Lausanne, 2023.
[23] EN 197-1: Cement - Part 1: Composition, specifications and conformity criteria for common cements, European committee for standardization, Brussels, 2013.
[24] EN 206-1: Concrete - Specification, performance, production and conformity, European committee for standardization, Brussels, 2021.
[25] FprEN 1992-1-1 final draft: Eurocode 2 - Design of concrete structures - Part 1-1: General rules and rules for buildings, bridges and civil engineering structures, European committee for standardization, Brussels, 2023.
[26] EN 12350-2: Testing fresh concrete – Part 2: Slump test, European committee for standardization, Brussels, 2019
[27] EN 12390-3: Testing hardened concrete - Part 3: Compressive strength of test specimens, European committee for standardization, Brussels, 2019.
[28] EN 14630: Products and systems for the protection and repair of concrete structures - Test methods - Determination of carbonation depth in hardened concrete by the phenolphthalein method, European committee for standardization, Brussels, 2006.
[29] A. Radović, V. Carević, A. Radević, B. Stupar, D. Veličkov, Influence of curing period on some mechanical and durability-related properties of limestone powder concrete, Gradjevinski materijali i konstrukcije (Building Materials and Structures) 67 (2024), 2400007R, https://doi.org./10.5937/GRMK2400007R
[30] S. Lay, P. Schießl, Service Life Models, Growth Programme: Life Cycle Management of Concrete Infrastructures for Improved Sustainability (LIFECON), Technical Research Centre of Finland (VTT), 2013, pp. 169.
[31] C. Gehlen, Probability-based service life design of reinforced concrete structures, Reliability studies for prevention of reinforcement corrosion, 2016, pp. 106 (in German).

Građevinski materijali i konstrukcije
Building Materials and Structures
journal homepage: www.dimk.rs

http://doi.org/10.5937/GRMK2500003I UDK: 699.841(497.2)

Technical paper

Seismic fragility curves for integral concrete bridge in Bulgaria

Alexander Iliev[*1)], Dimitar Stefanov[1)]

[1)] *National Institute of Geophysics, Geodesy and Geography (Bulgarian Academy of Sciences)*

Article history

Received: 05 February 2025
Received in revised form: 09 April 2025
Accepted: 22 April 2025
Available online: 19 May 2025

Keywords

Bridge seismic capacity,
Integral bridge,
Capacity spectrum method (CSM),
Seismic fragility curves

ABSTRACT

The determination of seismic behavior is a major issue concerning civil engineers nowadays. The development of computer systems has led to an increasing use of various analytical approaches for determining the seismic response of buildings and structures.
This study employs the Capacitive Spectrum Method (CSM) as an indirect approach to calculate fragility curves. In it, the capacity of the structure is represented by the so-called capacity curve which shows the relationship between force and displacement and thus represents the expected response for a given seismic load.In this procedure, the seismic excitation is represented by the 5% elastic response spectrum for the respective location and return period of the seismic input.
The Capacitive Spectrum Method (CSM) is based on a direct graphical comparison of the structural capacity (capacitive curve) with the required reduced elastic demand spectrum.
In the current paper, the seismic capacity and fragility curves for the integral bridge case study were developed.
The so-called fragility models and the relative probabilities of reaching four levels of damage are defined. These curves are used to develop loss models of the built environment. The discrete damage probabilities can be used as input data for determining and estimating various losses and damages in structures.

1 Introduction

Today's engineering practice primarily uses numerical analyses to calculate the seismic capacity of civil structures. There are different options for representing both the structural model and the seismic motion/load. In this study, the structure of a reinforced concrete road integral bridge was analyzed using the “Finite Element Method” (FEM) and a group of nonlinear static analyses, taking into account the interaction with the ground base. The nonlinear static analysis gives a good idea of the failure mechanism (plastification zones) of structures loaded with horizontal loads. Its advantage over dynamic analysis is the significantly reduced computational time due to ignoring the dynamic part of the equation of motion. This type of analysis estimates the ultimate limit capacity of the structure well, but it fails to represent the development of damage at a different time from the seismic input.

More advanced methods need detailed analyses and better models, take more time, and are used to calculate individual structures, usually after simpler methods like screening procedures or for potentially dangerous facilities. They are not suitable for large earthquake projects where many structures need to be calculated.. Although fragility curves and probability damage matrices have traditionally been derived using observed data, recently there have been proposals to compile them using computational analyses. In this way, some of the shortcomings of empirical methods are overcome.

The Capacity Spectrum Method (CSM) is a modern method for determining the seismic behavior of a given structure for earthquakes of different intensities. Its use is increasingly gaining ground among practicing engineers due to a number of advantages it possesses. With the help of this method, the nonlinear behavior of structural elements in a given structure is more easily described. The method was first introduced in the document ATC-40 [1], and was subsequently slightly modified in FEMA-440 [2]. By means of the corresponding procedures, the response of a structure during a seismic action can be represented in a simple way. The Capacitive Spectrum Method (CSM) is based on a direct graphical comparison of the structural capacity (capacitive curve) with the required reduced elastic demand (seismic) spectrum.

This method assumes that the total maximum number of movements (both elastic and inelastic) of a complex system can be figured out by looking at the elastic response of a simpler system with just one degree of freedom, even though this simpler system has a different period and damping than the original. For the calculation of the effective damping β_{eff}

[*] Corresponding author:
E-mail address: eng.alexander.iliev@gmail.com

and appropriate reduction factors, it is necessary to represent the capacitive curve by its bi-linear approximation. Following the procedure from [1], the so-called "behavior point" of the studied structure for the selected seismic action is calculated.

In analytical methods, the development of damage in structural elements is obtained through static or dynamic nonlinear analysis.

The present study is a continuation of the previously calculated capacity curves [7] for the same reinforced concrete integral bridge. In the original work, nonlinear static analysis of the case study bridge were analyzed and push over curves based on different procedures in both horizontal directions were developed. In the present paper, the previously published results [7] are transformed in spectral displacement/acceleration format and a response assessment is made for a given seismic excitation.

2 Description of the case study concrete bridge

The case-study is a girder reinforced concrete frame bridge in straight and unsloped direction. The bridge consists of 3 spans and a total length of 40 m, Fig. 1. In the transverse direction, the bridge is 8.8 m in size, Fig. 2. The average height

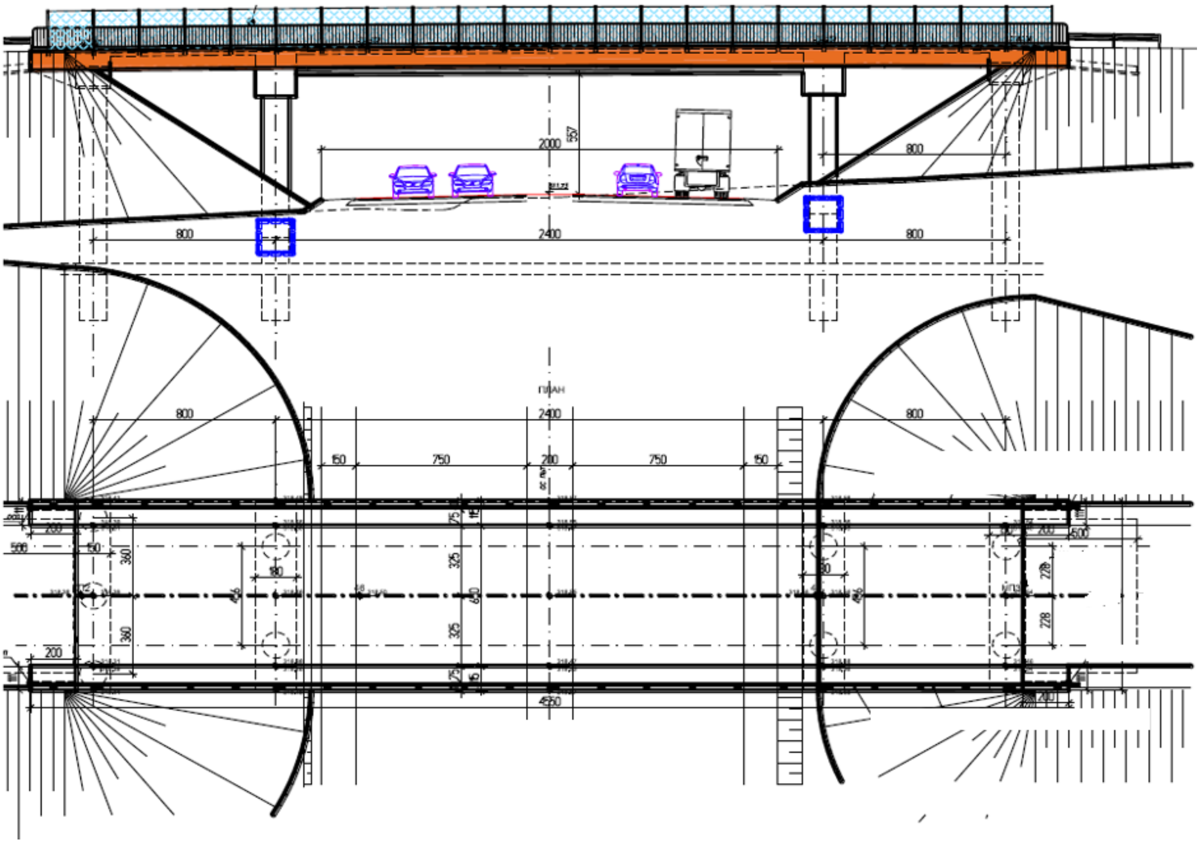

Fig. 1. Longitudinal and plan view of the bridge

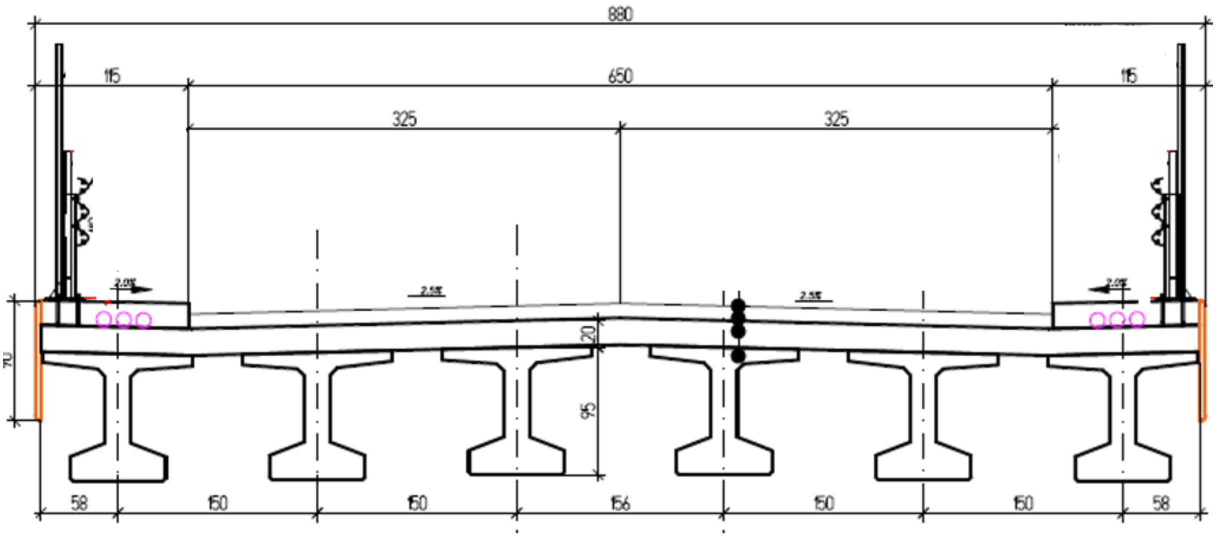

Fig. 2. Cross section of the middle span superstructure

of the columns is 6 m, and their diameter is 1.2 m. In the middle span (24 m) the longitudinal beams of the superstructure are prestressed. They are of the GT type and are 95 cm high. In the end spans, the superstructure is slab-shaped. A cross-section in the middle span of the overpass is shown in Fig. 2. The foundation is in a type C soil foundation, using cast-in-place piles with a diameter of 120 cm and a length of 22 m. The structure is designed with a significance factor of 1.4 and a behavior factor of 1.5. For loading from moving traffic, the LM1 load model [8] was adopted.

3 Assessment of the seismic response

To determine the seismic behavior (so-called performance point), it is necessary to present the capacitive spectrum and the demand (seismic) spectrum in the same format. The original nonlinear static push-over curve (Figure 3) was converted into the spectral displacement - spectral acceleration format. This transformation is done using the previously determined dynamic characteristics of the structure under study.

The intersection of the two spectra gives the so-called "performance point", which represents the response of the structure under study to the perceived seismic input (demand/seismic spectrum) - Fig. 4. In this case, the response of the structure is represented by the spectral displacement parameter - S_d .Subsequently, the fragility model is given for PGA earthquake parameter, since it gives a better applicability (“sense”) for further risk assessments. The numerical calculation of reduction coefficients in ATC-40 [1] is performed using formulas (1) and (2).

$$SR_A = \frac{3.21 - 0.68\ln\left(100\beta_{\text{eff}}\right)}{2.12} \quad (1)$$

$$SR_V = \frac{2.31 - 0.41\ln\left(100\beta_{\text{eff}}\right)}{1.65} \quad (2)$$

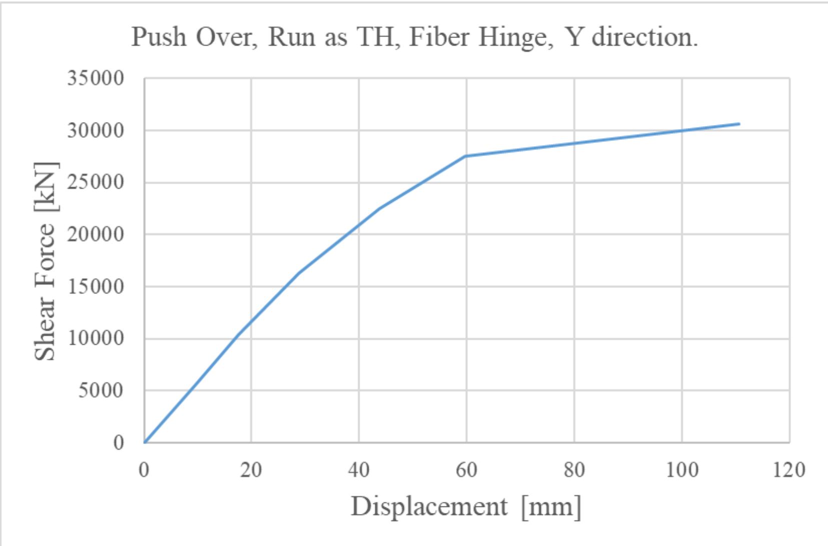

Fig. 3. Previously calculated push-over curve [7]

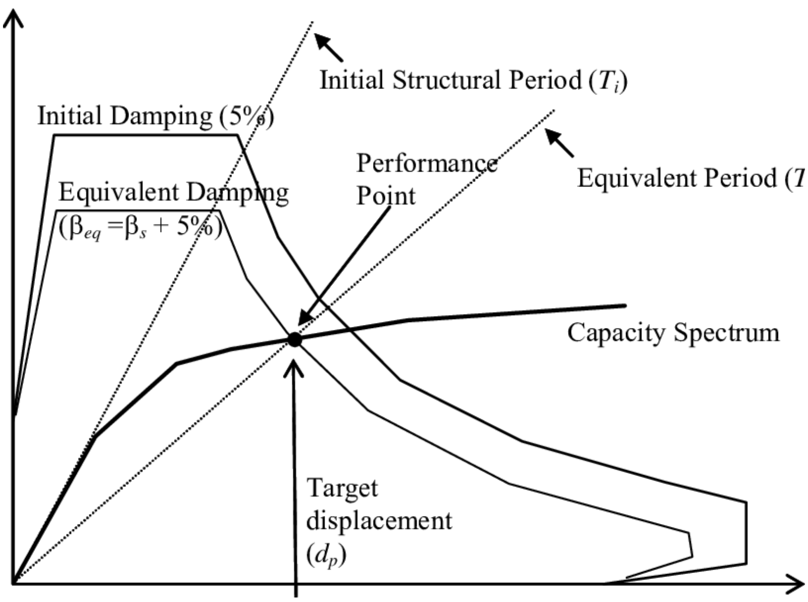

Fig. 4. Assessment of the performance point with CSM

For the initially selected point and the corresponding values for a_y, d_y, a_{pi} d_{pi} a β_{eff} value of 18% has been calculated. This corresponds to reduction factors $SR_A=0.59$ and $SR_V=0.69$, which reduce the initial demand elastic spectrum of the seismic action. Its intersection with the bi-linear capacity curve gives the temporary "behavior point" $a_{,int}/d_{,int}$– Fig. 5.

After lowering the demand (seismic) spectrum and intersecting it with the capacity spectrum, it should be determined whether the initially accepted behavior point a_p/d_p and the calculated behavior point a_{int}/d_{int} fulfill the convergence conditions. The initial point $a_{,p1}/d_{,p1}$ is considered suitable if it fulfills the criterion $0.95d_{,pi}<d_{int}<1.05d_{,pi}$. In this case, this requirement is not met, which is why a second iteration was performed with $a_{,p2}=1.81g/d_{,p2}=0.04m$, Fig. 6.

4 Definition of "Damage States"

Subsequently, for the purpose of determining conditional probabilities, the so-called "Damage States" are defined. They represent a discrete and qualitative description of the overall damage to structural and non-structural elements. Five damage levels are most commonly used: DS0 - No damage, DS1 – Light (Minor cracks or superficial damage to non-structural elements, such as surface coatings), DS2 – Medium (Noticeable structural damage, such as moderate cracking in critical components, slight deformation, or reduced functionality), DS3 –Severe (Significant structural compromise, including major cracks, deformation, or partial failure of key components, leading to restricted use) and DS4 – Destruction (Complete structural failure or collapse, rendering the bridge unusable and requiring full reconstruction).

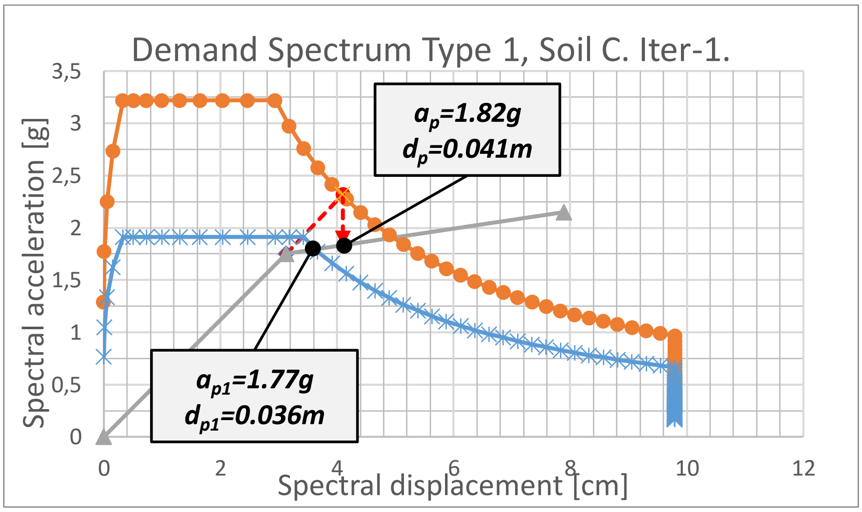

Fig. 5. Assessment of the initial performance point for PGA=0,8g (pointa_{pi}/d_{pi})

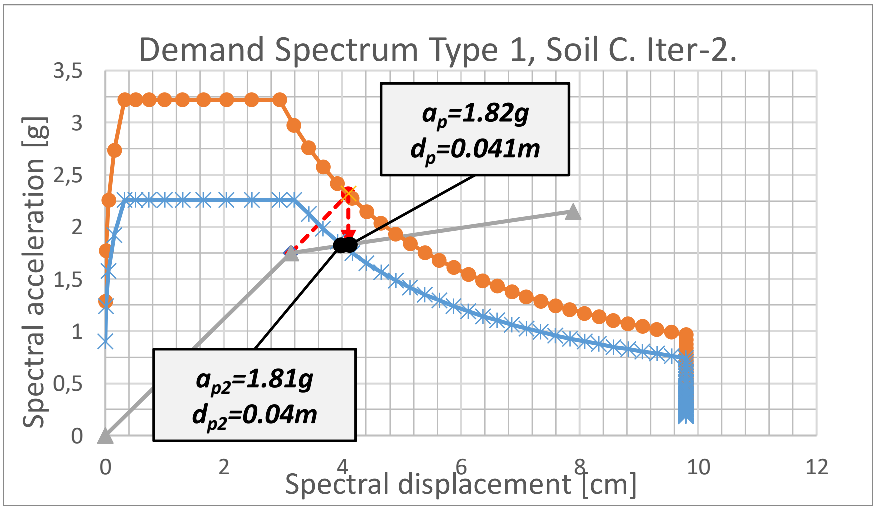

Fig. 6. Assessment of the performance point for PGA=0,8g (point a_{pi}/d_{pi}). Second iteration

The definition of damage levels (Table 1) can be done using the displacement values based on the capacity curve of the structure, [6].

Table 1. Definition of Damage States[6]

	Damage State	Limits of the spectral displacements
0	No damage	$D < 0.7^*D_y$
1	Light	$0.7^*D_y < D < D_y+1/3^*(D_u-D_y)$
2	Medium	$D_y+1/3^*(D_u-D_y) < D < D_y+2/3^*(D_u-D_y)$
3	Severe	$D_y+2/3^*(D_u-D_y) < D < D_u$
4	Destruction	$D > D_u$

5 Definition of fragility curves

The fragility model of a given structure (Fig. 7) consists of a group of fragility curves defining the conditional probability of reaching P[D=ds] or exceeding a certain level of damage P[D>ds].

Each fragility curve is defined by a median value of an impact parameter (spectral displacement) that corresponds to the limit of a given damage level and to the variability of the damage level. For example, the spectral displacement S_d, which defines the limit for a given level (ds), is calculated by the formula:

$$S_d=S_{d,ds}\times\varepsilon_{ds} \tag{3}$$

where:

$S_{d,ds}$ is the median value of the spectral displacement for the damage level, ds;

ε_{ds} is a lognormically distributed random variable with median value and logarithmic standard deviation, β_{ds}.

From the fragility curves thus defined and the calculated performance points for the respective seismic excitation (represented by a spectral displacement response parameter) the conditional probabilities for reaching or exceeding the respective damage level can be calculated.

For a given typology, the conditional probability of reaching a given level “DS” is represented by a cumulative lognormal function with respect to the spectral displacement at the corresponding "performance point".

$$P(DS|S_d)=\phi\left[\frac{1}{\beta_{DS}}\ln\left(\frac{S_d}{S_{d,DS}}\right)\right] \tag{4}$$

The fragility curves represent the distribution of damage at several levels of damage: Light, Medium, Severe and Destruction. For each given value of the spectral response, discrete probability values such as the difference of the cumulative probabilities of reaching or exceeding successive/related damage levels are calculated. The probability of reaching or exceeding different levels of damage for a given seismic level is 100%. Discrete probabilities of failures can be used for the determination and valuation of various losses and damages in structures.

There are different approaches for the treatment of uncertainties in the determination of seismic fragility. The most accurate results should be obtained when analyzing uncertainties using statistical methods for generating random samples of parameter values from a multidimensional distribution. The sampling method is often used to design computer experiments. This approach is quite laborious and requires handling large amounts of data. For this reason, tables with defined values of the relevant uncertainties for different types of structural typologies are presented in a number of manuals and documents.

Determining uncertainties in structural modeling is of primary importance for the probabilistic definition of seismic vulnerability. There are various sources of uncertainty, but the greatest importance should be given to uncertainties in the dissipation of input energy, uncertainties in the strengths of materials, as well as model uncertainties. Most often, uncertainties are described by normally distributed “Gaussian” functions, since they often give a very good representation of the distribution of the studied quantities.

One approach to determine the variability (uncertainties) of fragility curves is by applying f-li (5). In this, the variability is given as a function of the ductility of the structure under study. This approach has been implemented in the RISK-UE

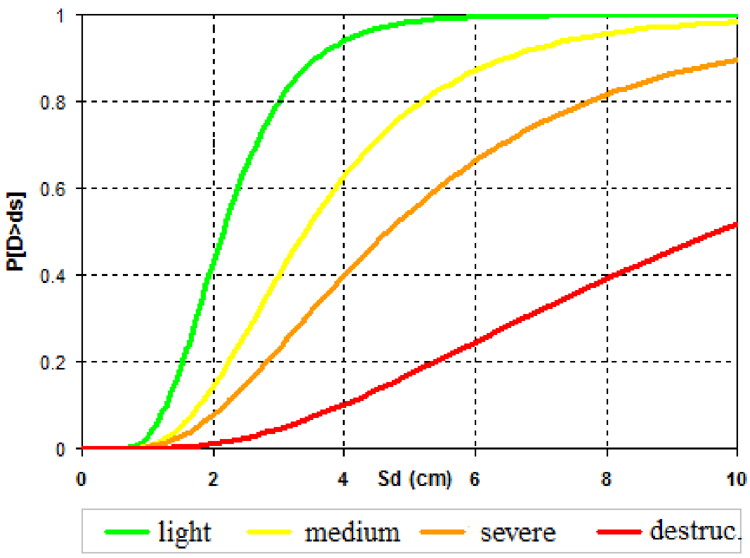

Fig. 7. Fragility model of given structure (fragility curves)

project [4] and provides a quick and easy way to calculate uncertainties in fragility curves through nonlinear static analysis.

$$\begin{aligned} \beta 1 &= 0.25 + 0.07 \ln \mu(u) \\ \beta 2 &= 0.2 + 0.18 \ln \mu(u) \\ \beta 3 &= 0.1 + 0.4 \ln \mu(u) \\ \beta 4 &= 0.15 + 0.5 \ln \mu(u) \end{aligned} \tag{5}$$

Subsequently, the numerical values necessary to define the damage levels for the studied structure are determined.

$S_{d,0}<0.7*S_{dy}=0.7*0.0313$ m=0.0125 m=>$S_{d,0}<2{,}19$ cm
$S_{d,1}>0.7*S_{dy}=0.7*0.0313$ m=0.0125 m=>$S_{d,1}>2{,}19$ cm
$S_{d,2}=S_{dy}+1/3(S_{du}-S_{dy})=3{,}13+1/3(7{,}9-3{,}13)=4{,}72$ cm
$S_{d,3}=S_{dy}+2/3(S_{du}-S_{dy})=1.79+2/3(7{,}9-3{,}13)=6{,}30$ cm
$S_{d,4}=S_{du}=0.079$ m=7,9 cm

After defining the fragility model (the group of curves), specific discrete values of the probabilities of damage occurrence due to a given seismic impact can be determined. In this case, the probabilities of reaching damage to the reinforced concrete bridge for a seismic input with a maximum ground acceleration PGA=0.8g have been determined. An input with such intensity corresponds to a spectral displacement of 4.0 cm. Fig. 8 presents the obtained relative probabilities of reaching the four levels of damage (light, medium, severe, destruction), through uncertainties determined by formulas (5).

To have a better understanding and applicability for risk assessment purposes, the fragility model is also calculated in PGA format. This is more convenient in certain cases as PGA gives a direct understanding of the earthquake event.

The performance point is calculated with a certain simplification for the damping (β_{eff}) value to 5% (elastic response) for different earthquake levels (demand spectra). In reality, for higher earthquake scenarios, due to dissipation of the structure due to damage, the damping value will be higher.Its intersection with the bi-linear capacity curve gives the“behavior point” for four seismic levels (damage states)$a_{,int}/d_{,int}$– Fig. 9.

Finally, the fragility model is calculated for four damage levels in terms of PGA values, Fig. 10.

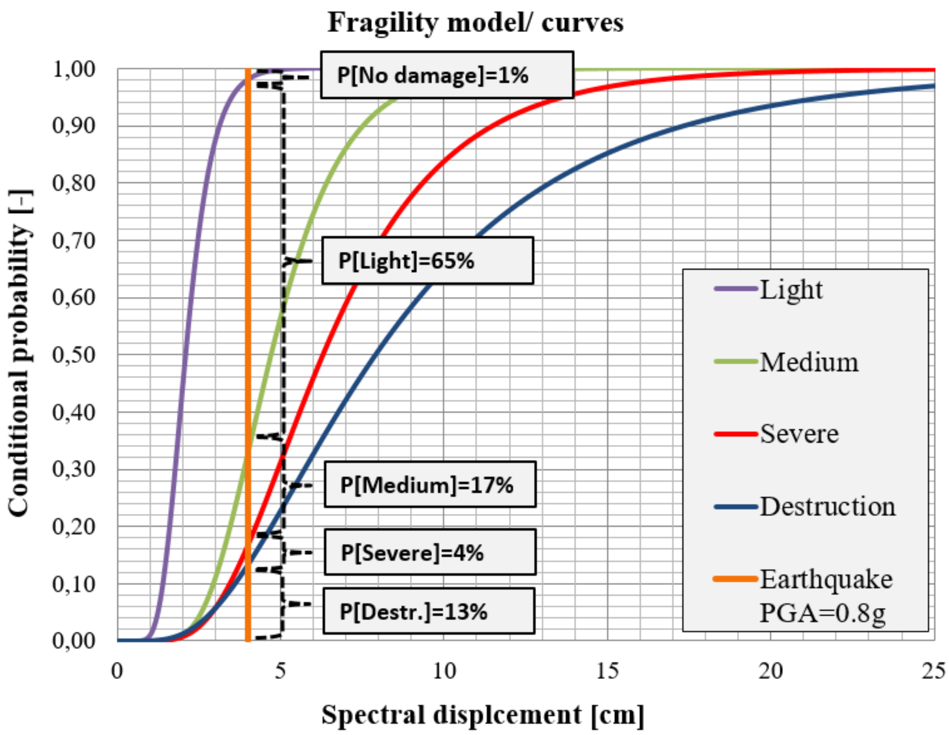

Fig. 8. Fragility model giving the relative probabilities of damage

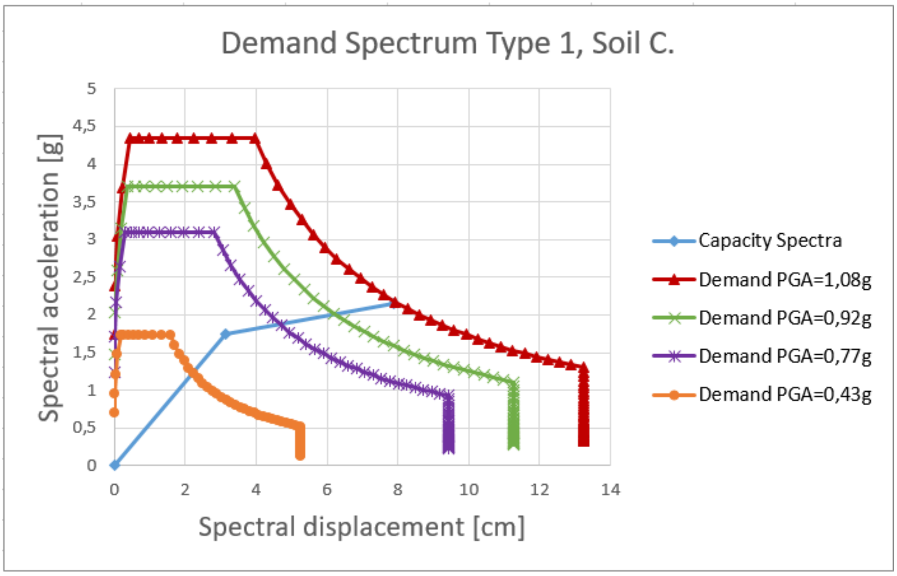

Fig. 9. Assessment of the performance point for different PGA levels (seismic events)

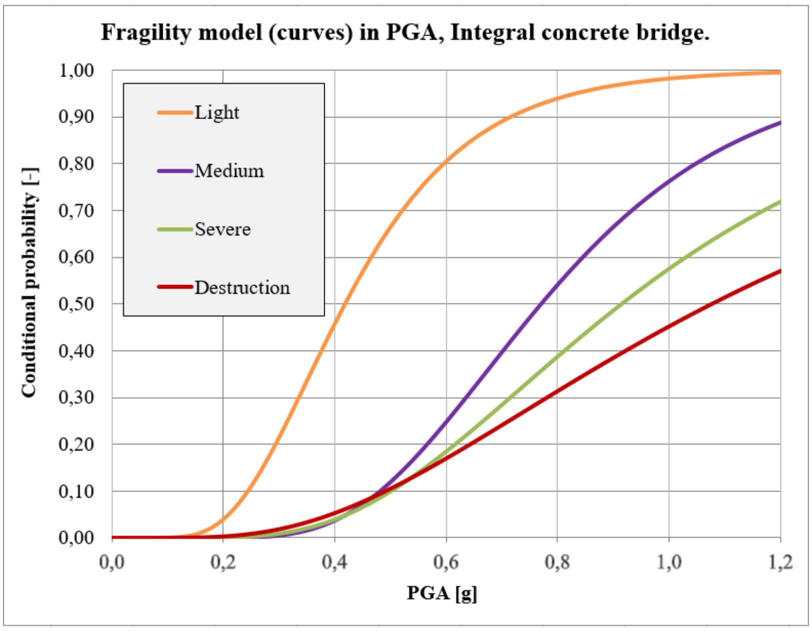

Fig. 10. Fragility model giving the relative probabilities of damage (in PGA)

6 Conclusions

In this study, the seismic response of a reinforced concrete integral bridge structure is analyzed using the Capacity Spectrum Method, taking into account the soil-structure interaction (SSI) through seismic spectra for soil class C and elastic springs for piles, calculated based on [9]. Its advantage over dynamic analysis is the significantly reduced computational time due to ignoring the dynamic part of the equation of motion. This type of analysis estimates the ultimate limit capacity of the structure well, but it fails to represent the development of damage at a different time from the seismic input.

The estimated failure scenarios are presented along with the accumulated damage and deformations in the structure. Subsequently, the so-called fragility model and the conditional probabilities for reaching four levels of damage are defined. For the studied seismic excitation (catastrophic earthquake) with a maximum peak ground acceleration PGA = 0.8 g, it is most likely that "light" to "medium" damage will occur in the structure. This indicates the very good seismic capacity of the newly designed facilities according to current modern regulatory documents (Eurocode). Discrete damage probabilities can be used as input data for the determination and valuation of various losses and damages in the structures.

CRediT authorship contribution statement

Alexander Iliev: Writing- original draft, Formal Analysis, Resources, Visualization, Methodology.

Dimitar Stefanov: Writing-review & editing, Conceptualization, Resources, Validation, Supervision.

Declaration of competing interest:

The authors declare that they have no known competing financial interests or personal relationships that could have appeared to influence the work reported in this paper.

Acknowledgments

This study was conducted without any external support.

Literature

[1] AppliedTechnology Council(ATC-40), Seismic Evaluation and Retrofit of Concrete Buildings, California, U.S.A, 1996.

[2] Applied Technology Council (FEMA-440). Improvement of Nonlinear Static Seismic Analysis Procedures,California, U.S.A, 2005.

[3] Grünthal G., Cahiers du Centre Européen de Géodynamique et de Séismologie: Volume 15 – European Macroseismic Scale 1998. European Center for Geodynamics and Seismology, Luxembourg, 1998.

[4] RISK- EU, The European Risk-Ue Project: An Advanced Approach to Earthquake Risk Scenarios (2001-2004) www.risk-ue.net.

[5] Federal Emergency Management Agency(HAZUS), Earthquake Loss Estimation Methodology - Technical and User Manuals., Washington, D.C, 1998.

[6] Ioannis F. Moschonas, Andreas J. Kappos, Panagiotis Panetsos, Vissarion Papadopoulos, Triantafyllos Makarios, Pavlos Thanopoulos - Seismic fragility curves for Greek bridges: methodology and case studies, Bull Earthquake Eng, 2009.

[7] A.Iliev, D.Stefanov, P.Nikolov- Nonlinear Static (Push-Over) Analysis of Integral Concrete Bridge. Scientific Journal 'Mechanics Transport Communications', Issue: 2 / 2024.

[8] EN 1998-2, Eurocode 8: Design of structures for earthquake resistance, Part 2: Bridges.

[9] Priestley, M.J.N, Seible F and Calvi G.M., Seismic Design and Retrofit of Bridges, John Wiley & Sons, p.465, 1996.

Građevinski materijali i konstrukcije
Building Materials and Structures
journal homepage: www.dimk.rs

https://doi.org/10.5937/GRMK2500005S UDK: 624.21(549)

Technical paper

Reliability analysis of prestressed concrete bridges under prevailing truck traffic in Pakistan

Hamza Shams*[1], Yanjun QIU*[1], Muhammad Kashif[2], Hanif Ullah[3], Hamid Abdrhman[1], Jianfeng FU[4], Enhui Yang[1]

[1] *Highway Engineering key Lab of Sichuan Province, School of Civil Engineering, Southwest Jiaotong University, Chengdu 610031, China*
[2] *School of Civil Engineering, Southwest Jiaotong University, Chengdu 610031, China*
[3] *Department of Civil & Environmental Engineering, King Fahd University of Petroleum and Minerals, Eastern Province, Saudi Arabia*
[4] *Sichuan Mianjiu Expressway CO., LTD., Mianyang, Sichuan, 621000, China*

Article history

Received: 14 April 2025
Received in revised form: 23 May 2025
Accepted: 27 May 2025
Available online: 13 June 2025

Keywords

Bridge reliability,
prestressed concrete,
truck traffic,
live load models,
structural safety,
Pakistan,
AASHTO LRFD,
PHB Code

ABSTRACT

This paper presents a comprehensive reliability assessment of prestressed concrete bridges in Pakistan subjected to prevailing truck traffic conditions. The study compares actual load effects from weigh-in-motion (WIM) data with design specifications from the Pakistan Highway Bridge (PHB) Code (1967) and AASHTO LRFD. Statistical analysis of axle weights, configurations, and gross vehicle weights (GVW) reveals that 72.7% of trucks exceed legal load limits, with 5-axle trucks showing 97% non-compliance. Reliability analysis using First-Order Second Moment (FOSM) methods indicates that existing bridge designs exhibit significant variations in safety margins, with reliability indices (β) ranging from 2.51 (Chitral Bridge) to 5.6 (Bannu Road Bridge). The results demonstrate that current design codes do not accurately represent Pakistan's truck traffic, leading to potential overstressing or underutilization of bridges. The study recommends revising live load models based on empirical traffic data and implementing stricter enforcement of weight regulations to enhance bridge safety and longevity.

1 Introduction

The development of accurate live load models for bridge design represents a critical intersection between structural reliability theory and transportation engineering practice. Contemporary research has demonstrated that the probabilistic characterization of traffic loads constitutes the most uncertain component in bridge reliability analysis [1]. The evolution of live load modeling has progressed significantly since the early deterministic approaches, with current methodologies emphasizing site-specific calibration using Weigh-in-Motion (WIM) data and extreme value statistics [2]. The AASHTO LRFD specifications [3], derived from extensive WIM studies conducted in North America during the 1980s and 90s [4], represent a landmark achievement in reliability-based bridge design. However, as highlighted by Caprani et al. [5], the direct application of these models to developing countries often leads to significant discrepancies due to variations in truck configurations, enforcement practices, and traffic growth patterns.

Recent advances in structural reliability theory have enabled more sophisticated treatment of live load uncertainties. Melchers, Robert E., and André T. Beck [6] have shown that modern Bayesian updating techniques can effectively incorporate WIM data into time-dependent reliability assessments, particularly for bridges subjected to increasing traffic volumes. This is especially relevant for Pakistan's context, where studies by Hafeez et al. [7] have documented alarming trends in truck overloading, with gross vehicle weights frequently exceeding legal limits by 30-50%. The situation mirrors challenges observed in other developing nations, where Ghosh et al. [8] reported similar discrepancies between code-specified loads and actual traffic conditions in Brazil and India.

The reliability assessment of prestressed concrete bridges presents unique challenges due to the time-dependent nature of prestress losses and material degradation. Fan, Ziyuan, et al [9] developed a comprehensive framework for incorporating these effects into reliability analysis, demonstrating that conventional safety factors may become unconservative over extended service periods. This finding is particularly pertinent to Pakistan's bridge inventory, where many structures designed to the outdated PHB Code [10] now face traffic loads far exceeding original assumptions. Statistical handling of traffic data, such as axle weight and configuration, plays a significant role in determining the loads carried on bridges. This may indicate non-adherence to regulatory load requirements, as seen in Pakistan's truck traffic analysis [11].

* Corresponding author:
E-mail address: hamza.shams97@gmail.com; publicqiu@vip.163.com;

Emerging research has also highlighted the importance of considering multiple presence effects in reliability analysis, particularly for medium-span bridges standard in Pakistan's highway network. Žnidarič et al. [12] demonstrated that ignoring vehicle interaction effects can lead to underestimation of maximum load effects by 15-20%. This oversight becomes increasingly significant as traffic densities rise, a trend well-documented in Pakistan's recent transportation studies [13]. The current study addresses this gap by employing First-Order Second Moment (FOSM) methods while acknowledging the need for more sophisticated analysis in future work.

The literature reveals a clear imperative for Pakistan to develop its reliability-based design framework, building on international best practices while accounting for local traffic characteristics. As demonstrated by the European Union's successful implementation of region-specific load models [14], such an approach can achieve an optimal balance between safety and economy. This study contributes to this objective by providing the first comprehensive reliability assessment of Pakistani bridges using actual traffic data, filling a critical gap identified in recent reviews of developing country infrastructure [15].

In this study, two types of bridges were considered. For reliability analysis, single-loaded events were considered, while multiple presence effects were ignored. Code-specified girder distribution factors (GDF) for moment and shear were used from respective codes, which gives conservative results. Statistical characteristics (Mean and Coefficient of variation) for dead load (DL) and impact load (IM), resistance (R), and GDF were taken from previous research on the subject.

2 Research aim and objectives

The reason for this study is to really take a look at the sufficiency of different types of bridges based on the service-level truck traffic passing over the bridges with a view to generate essential data for developing live load safety factors for the design of bridges in Pakistan. The specific objectives are:

- Statistical characterization of live load effects (shear and moments) under service-level truck traffic passing over the bridges.
- Statistical projection of the live load effect to 75 years for estimating the mean maximum load effect.
- Check the adequacy of different types of bridges under the actual truck traffic passing over the bridges through reliability analysis.

3 Research methodology

This study employs a rigorous, multi-faceted research methodology to evaluate the reliability of prestressed concrete bridges in Pakistan under actual truck traffic conditions. The approach integrates empirical data collection, advanced statistical analysis, and structural reliability theory, aligning with international best practices while addressing Pakistan-specific challenges.

The study begins with a critical review of existing bridge design codes, including the outdated Pakistan Highway Bridge (PHB) Code [10] and the modern AASHTO LRFD specifications [3]. This comparison highlights potential gaps between design assumptions and real-world conditions.

The methodology draws on international research to contextualize Pakistan's challenges within broader trends in developing countries, such as truck overloading and code discrepancies.

3.1 Data Collection and Characterization

3.1.1 Bridge Inventory and Selection

- Representative Sampling: Bridges are selected based on span length, geometry, and material properties to ensure a representative sample (e.g., Chitral Bridge and Bannu Road Bridge).
- Structural Parameters: Key data include girder dimensions (flange widths, web heights), concrete strengths (28–35 MPa), and prestressing details, sourced from design documents and field measurements.

3.1.2 Traffic Load Data

- Weigh-in-Motion (WIM) Systems: Empirical truckload data (axle weights, configurations, Gross vehicle weight(GVW)) are collected via mobile weighing stations, capturing real-time traffic patterns.
- Statistical Characterization: Axle load distributions, coefficients of variation (COV), and extreme values are analyzed. Findings reveal that 72.7% of trucks exceed legal limits, with 5-axle trucks showing 97% non-compliance.

3.1.3 Load Effects Calculation

- Shear and Moment Demands: Load effects are computed for actual truck traffic using influence line analysis, comparing results with PHB Code and AASHTO LRFD predictions. Discrepancies of 15–30% are identified, underscoring code inadequacies.

3.2 Reliability Analysis

3.2.1 Resistance Modeling

- Material and Geometric Variability: The Resistance (R) of prestressed girders is modeled using statistical parameters (bias factors λ and COV) derived from prior research (e.g., λ = 1.05 for moment resistance, COV = 0.075) [16].
- Limit States: Focus on moment and shear capacity, accounting for time-dependent prestress losses and concrete degradation.

3.2.2 Load and Resistance Interaction

- First-Order Second Moment (FOSM) Method: Reliability indices (β) are calculated using FORM (First-Order Reliability Method), with:
  - Load (Q): Mean (μ_0) and standard deviation (σ_0) from WIM data.
  - Resistance (R): Nominal values (R_n) adjusted for bias and variability.
- Comparative Analysis: Two load combinations are evaluated:
  1. AASHTO LRFD: 1.25(DC) + 1.5(DW) + 1.75(LL+IM)
  2. PHB Code: 1.5(DL) + 2.5(LL+IM)

where:

AASHTO = American Association of State Highway and Transportation Officials
LRFD = Load and Resistance Factor Design
DC = Dead load of the component
DW = Dead Load of weight of the structure
LL = Live Load
IM = Impact Load.

3.2.3 Reliability Index (β) Calculation

• Target Benchmarking: Results are compared against AASHTO LRFD's target β of 3.5 for strength limit states.

a) Chitral Bridge: β = 2.51 (below target, indicating under-design).
b) Bannu Bridge: β = 5.6 (overly conservative, suggesting cost inefficiencies)

3.3 Validation and Sensitivity Analysis

• Cross-Referencing with Global Studies: Results are validated against findings from similar contexts, confirming trends in overloading and reliability gaps.

• Parametric Studies: The Sensitivity of β to variables like span length (shorter spans show higher live-load sensitivity) and girder geometry (e.g., web height, flange width) is assessed.

3.4 Projection to 75-Year Service Life

• Extreme Value Statistics: Maximum load effects over a 75-year design life are estimated using statistical extrapolation techniques, ensuring long-term safety assessments.

4 Results and discussion:

The study presents a critical reliability assessment of prestressed concrete bridges in Pakistan, comparing actual truckload effects with design specifications from the Pakistan Highway Bridge (PHB) Code [10] and AASHTO LRFD [3]. The findings highlight significant discrepancies between code-based live load models and empirical truck traffic data, raising concerns about structural safety and economic efficiency.

Figure 1 compares average and maximum truckloads from mobile weighing stations with NHA permissible limits. The data shows that 72.7% of trucks exceed legal limits, with 5-axle trucks exhibiting 97% non-compliance. This trend is consistent with studies in other developing nations, where lax enforcement and economic pressures lead to chronic overloading [17]. For instance, in India, WIM data revealed that 65–80% of trucks exceeded legal axle loads, accelerating bridge deterioration [18].

Figure 2 (Peshawar Development Authority (PDA) Data) illustrates the discrepancy between actual and code-specified load effects. The shear and moment demand from 5-axle trucks exceed PHB Code predictions by 15–30%, mirroring findings in Brazil, where live load models underestimated real traffic effects by 20–25% [19].

Figure 3 highlights extreme cases where maximum recorded loads surpass NHA limits by 40%. Such overloading is comparable to observations in South Africa, where overloaded trucks reduced bridge service life by 30–50% [20].

Tables 1 (PDA Data) provide granular axle weight distributions, revealing that:

• Single-unit trucks (3-axle) are 25% heavier than legal limits.

• Tractor-trailers (5-axle) show higher variability (COV = 0.35), indicating inconsistent loading patterns.

These findings align with Nowak et al. [4], who emphasized that traffic variability must be incorporated into live load models to ensure accurate safety assessments.

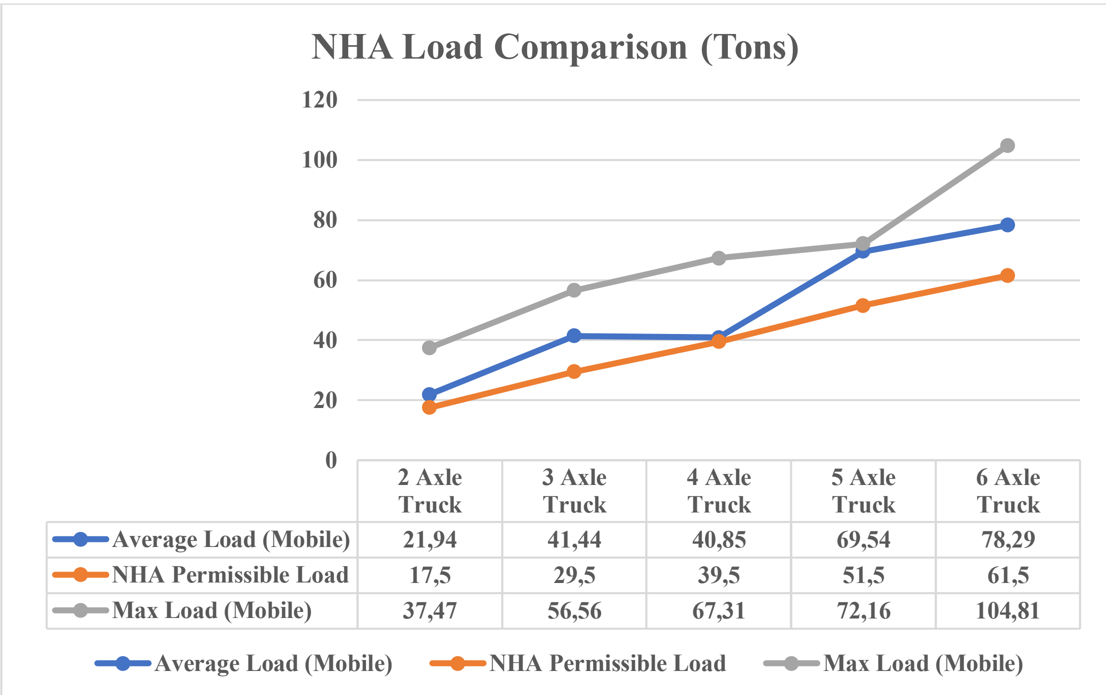

NHA (National Highway Authority)

Figure 1. Comparison of average load of mobile weighting station Vs NHA permissible load and Maximum loads of mobile weighting station

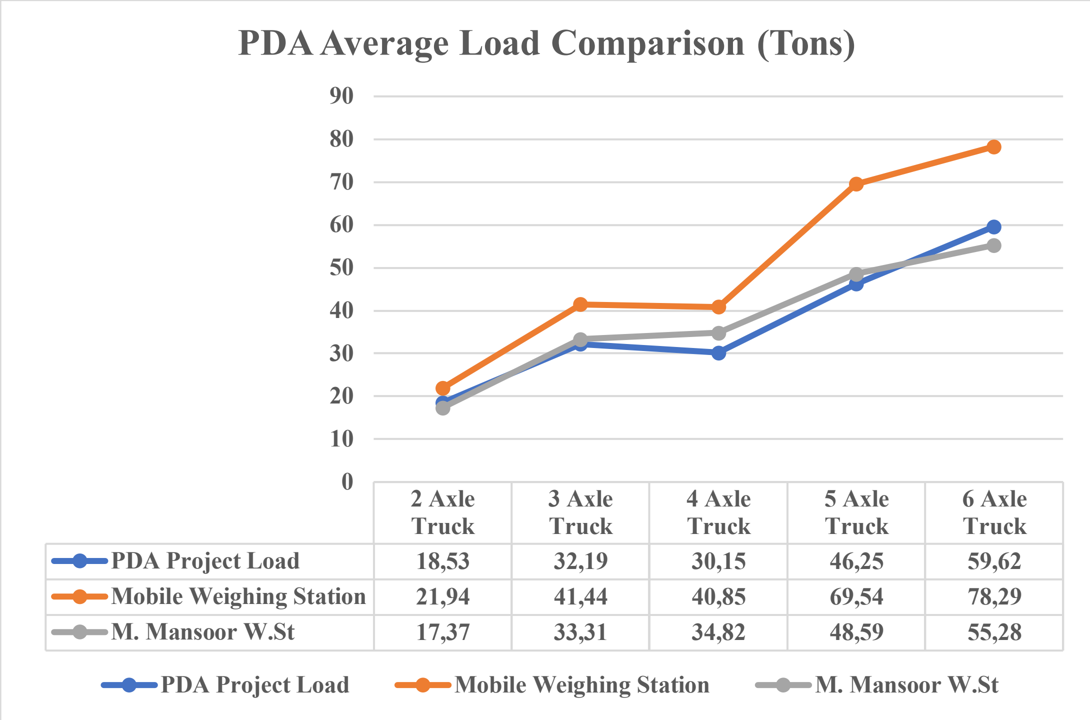

	2 Axle Truck	3 Axle Truck	4 Axle Truck	5 Axle Truck	6 Axle Truck
PDA Project Load	18,53	32,19	30,15	46,25	59,62
Mobile Weighing Station	21,94	41,44	40,85	69,54	78,29
M. Mansoor W.St	17,37	33,31	34,82	48,59	55,28

PDA (Peshawar Development Authority), M.MansoorW.St (Muhammad Mansoor Weight Station)

Figure 2. Load Comparison (PDA)

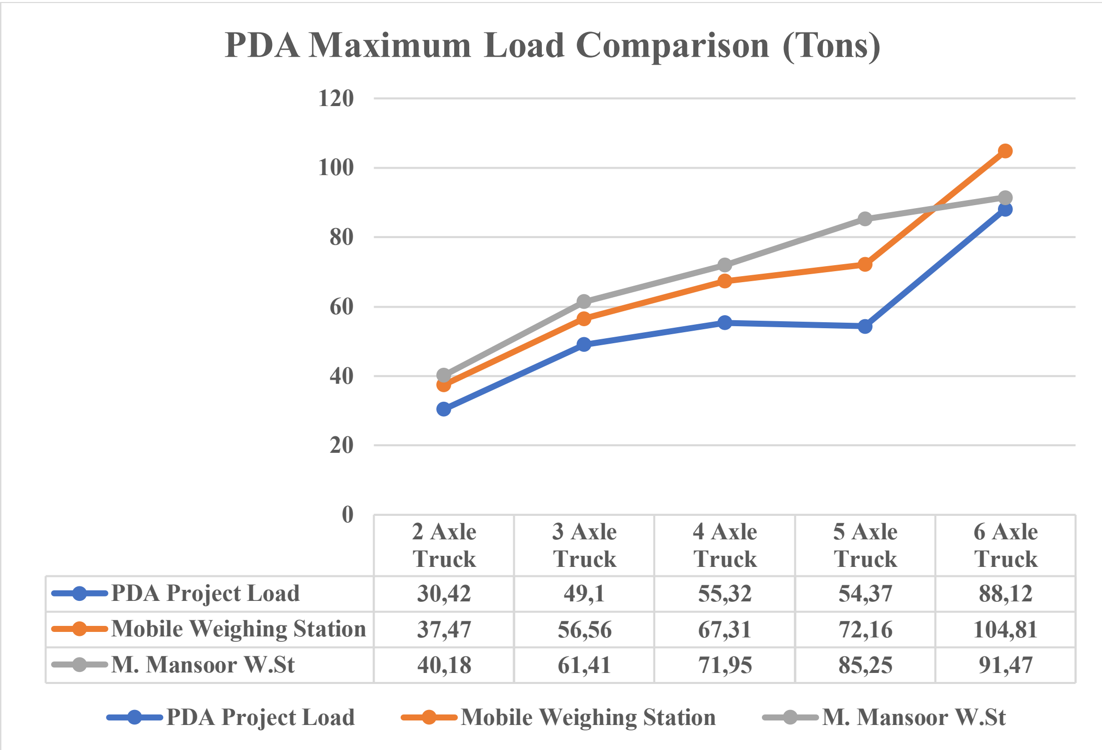

	2 Axle Truck	3 Axle Truck	4 Axle Truck	5 Axle Truck	6 Axle Truck
PDA Project Load	30,42	49,1	55,32	54,37	88,12
Mobile Weighing Station	37,47	56,56	67,31	72,16	104,81
M. Mansoor W.St	40,18	61,41	71,95	85,25	91,47

PDA (Peshawar Development Authority), M.MansoorW.St (Muhammad Mansoor Weight Station)

Figure 3. Maximum Load Comparison

Table 1. Load data provided by PDA

Tractor With Trolley	2 Axle	3 Axle	4 Axle	5 Axle	6 Axle
20%	47%	17%	4%	3%	9%

4.1 Reliability analysis

4.1.1 Resistance Model:

The capacity of a bridge to withstand load mainly depends upon the resistance(R) of its components, which is a function of its material properties, section geometry, and dimensions. Table 2 below shows the statistical parameters for the resistance components of the prestressed concrete girder.

4.1.2 Reliability Index (β)

The reliability analysis in this study is based on the safety index calculation, also called the Reliability index (β). The reliability index is defined as the function of the probability of failure. The Equation can be written as;

$$\beta = \frac{R_n\lambda_R(1-KV_R)[1-\ln(1-KV_R)]-\mu_Q}{\sqrt{\{[R_n\lambda_R V_R(1-KV_R)]^2+(б_Q)^2\}}}$$

where;

R_n = Nominal Resistance 55
λ_R = Bias of Resistance
K = Measure of shift from mean value in standard deviation units, assumed
V_R = COV of Resistance
μ_Q = Mean of total load or load effects
$б_Q$ = Standard deviation of total load or load effects

For strength one limit state equation can be written as

Q (AASHTO) = 1.25 (DC1 + DC2) + 1.5 DW + 1.75(LL + IM)

where;

DC1 = Dead Load of component 1
DC2 = Dead Load of component 2
DW = Dead Load of weight of the structure
LL = Live Load
IM = Impact Load

For pre-stressed design, the equation as given in PHB code 1967 is;

Q (PHB Code) = 1.5 DL + 2.5 (LL + IM)

where;

PHB = Preliminary Highway Bridge Code
DL = Dead Load
LL = Live Load
IM = Impact Load

The safety index (β) for pre-stressed girders has only been calculated considering supported sample bridges using the above equation for both codes separately.

4.1.3 Sample Bridges

Two bridges, along with their parameters, are selected for the analysis, as shown in Figure 4 and Table 3 below:

Table 2. Statistical Parameters for Resistance Components of Prestressed Concrete Girders

Component	Limit State	Bias Factor (λ)	COV(V)
Material/Fabrication	Moment	1.04	0.045
	Shear	1.07	0.10
Professional Factor	Moment	1.01	0.06
	Shear	1.075	0.10
Resistance (R)	Moment	1.05	0.075
	Shear	1.15	0.14

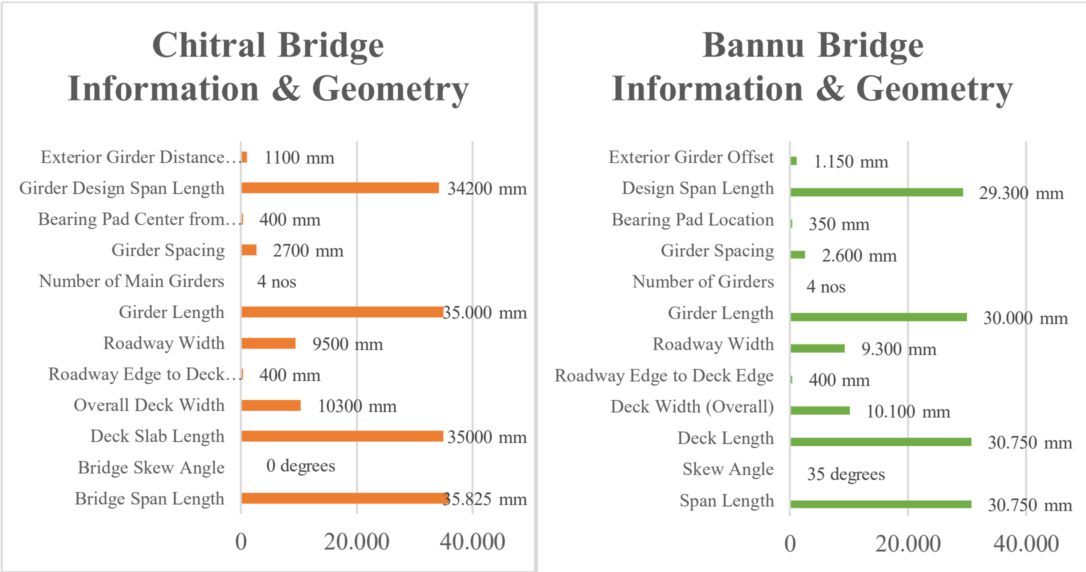

Figure 4. Chitral and Bannu Bridge Information

Table 3. Properties of Materials of Chitral & Bannu Bridge

Parameter	Chitral Bridge Values	Bannu Bridge Values	Unit
Girder Concrete Strength:			
At service state	35	35	MPa
At the time of Prestressing	28	28	MPa
Deck Slab Concrete Strength	35	35	MPa

A reliability analysis of two of the above bridges was conducted based on their capacity (resistance), total load effects (mean actual load), and other required coefficients and factors.

The reliability analysis conducted for the Chitral Bridge (CB) and Bannu Road Bridge (BRB 45+400) provides critical insights into the safety margins of these structures under specified load and resistance conditions. The results are summarized in Table 4, with reliability indices (β) of 2.51 (Chitral Bridge) and 5.6 (Bannu Bridge), respectively. These values are derived from the First-Order Reliability Method (FORM), considering the statistical parameters of load and resistance. These values are benchmarked against AASHTO LRFD's target β of 3.5 for strength limit states.

The Chitral Bridge exhibits a β of 2.51, which falls below the typical target range of 3.0–3.5 for bridges under strength limit states, as recommended by Nowak et al. [1] and AASHTO LRFD specifications [3]. This suggests a potential under-design or higher vulnerability to failure. The results are consistent with bridges in Nigeria, where outdated codes led to β < 3.0 [21].

In contrast, the Bannu Road Bridge achieves a β of 5.6, significantly exceeding the target. This indicates an overly conservative design, possibly leading to unnecessary material use and cost inefficiencies. Studies in the U.S. suggest that β > 4.5 often indicates excessive safety margins, increasing costs without proportional benefits [22].

Chitral Bridge resistance (R) distribution overlaps significantly with load effect (Q), confirming its low β. This aligns with [23], who found that β < 3.0 correlates with premature fatigue cracking. Bannu Road Bridge's wide gap between R and Q explains its high β, resembling over-designed bridges in Europe [5].

Both bridges share identical mean applied load (μ_0 = 6,132.34 KN-m) and coefficient of variation (V_0 = 0.195) for loads, derived from Weigh-in-Motion (WIM) data. However, the Bannu Bridge's higher nominal resistance (R_n = 20,700 KN-m vs. 15,000 KN-m for Chitral) and similar bias factor (λ_r = 1.05) and COV (V_r = 0.075) contribute to its superior reliability.

The resistance model's bias factors and COV values align with established literature. For instance, Nowak et al. [24] reported typical bias factors of 1.03–1.09 and COVs of 0.06–0.12 for prestressed concrete girders, corroborating the study's assumptions.

- **Shorter spans (<20 m)** exhibit lower β due to higher live-load sensitivity, as observed in Nowak's (1993) U.S. bridge surveys.
- **Pre-stressed concrete girders** show lower COV in resistance (0.10–0.15) compared to steel (0.20–0.25), supporting their reliability advantages [2].

Table 4. Reliability Index Calculation for Chitral and Bannu Bridge (75 Years)

Parameter	Symbol	Chitral Bridge Value	Bannu Bridge Value	Unit	Notes
Design Life	-	75	75	years	
Span Length	L	35	30.00	m	Supported span
Load Characteristics					
Mean applied load	μ_0	6,132.34	6,132.34	KN-m	From WIM data
Standard deviation of load	σ_0	3,358	3,358.00	KN-m	
Coefficient of variation (load)	V_0	0.195	0.195 (19.5%)	-	σ_0/μ_0
Resistance Characteristics					
Nominal resistance	R_n	15,000	20,700	KN-m	Design value
Bias factor of resistance	λ_r	1.05	1.05	-	Mean/nominal ratio
COV of resistance	V_r	0.075	0.075 (7.5%)	-	Material variability
Reliability Analysis					
Calculated Reliability Index	β	2.51	**5.6**		Calculated via FORM

The Chitral Bridge's girder geometry (e.g., web height = 1,140 mm) and material strengths (35 MPa concrete) are comparable to those of the Bannu Bridge (web height = 1,350 mm, 35 MPa concrete). However, the Bannu Bridge's more considerable span length (30 m vs. 35 m for Chitral) and optimized girder dimensions (e.g., wider top flange: 900 mm vs. 800 mm) likely enhance its resistance capacity, as noted in Table 5. The Girder layout is shown in Figure 5.

Table 5. Geometry of Chitral Bridge and Bannu Bridge Girders

Parameter Description	Symbol	Chitral Bridge Values	Bannu Bridge Values	Unit	Visual Reference
Top Flange Width	W1gir	800	900	mm	[Top Flange]
Top Flange Thickness	T1gir	205	130	mm	
1st Triangle (Top) Width	W2gir	310	250	mm	[Triangle 1]
1st Triangle (Top) Height	T2gir	155	70	mm	
2nd Triangle (Top) Width	W3gir	100	100	mm	[Triangle 2]
2nd Triangle (Top) Height	T3gir	100	100	mm	
Middle Web Width	W4gir	180	200	mm	[Web]
Middle Web Height	T4gir	1,140	1,350	mm	

Triangle (Bottom) Width	W5gir	210	200	mm	[Triangle 3]
Triangle (Bottom) Height	T5gir	210	200	mm	
Bottom Flange Width	W6gir	600	600	mm	[Bottom Flange]
Bottom Flange Thickness	T6gir	290	250	mm	

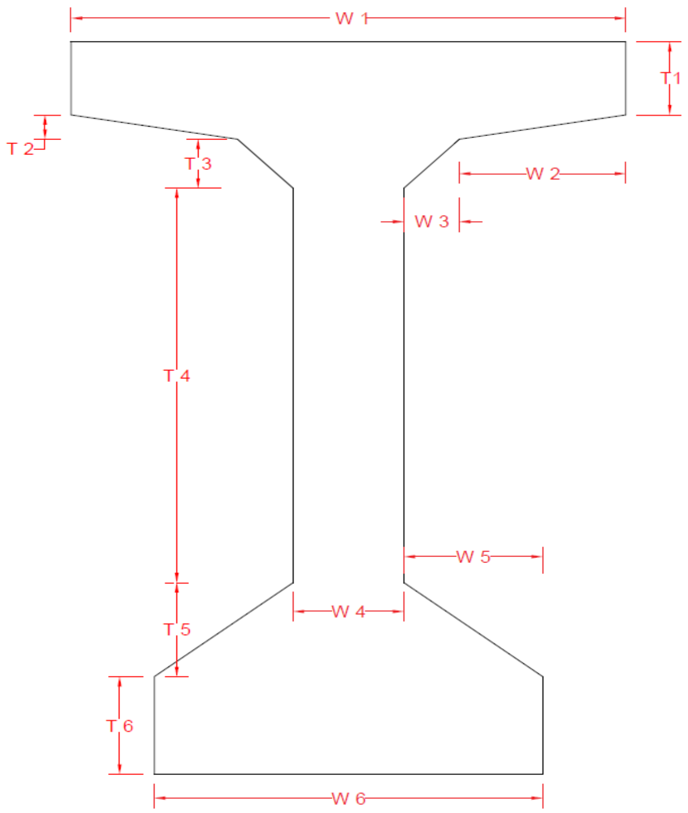

Figure 5. Girder Layout

The study contrasts two load combinations: AASHTO LRFD (Q = 1.25 (DC) + 1.5 (DW) + 1.75 (LL+IM)) and the older PHB Code (Q = 1.5 (DL) + 2.5 (LL+IM))). The PHB Code's higher live load factor (2.5) may explain the Bannu Bridge's elevated β, reflecting historical conservatism. Modern codes like AASHTO LRFD aim for balanced safety without excessive over-design [25]. Table 6 shows the data of Bannu and Chitral bridge for better comparison.

Table 6. Integrated Structural, Material, Reliability, and Girder Geometry Data for Chitral and Bannu Bridges

Parameter	**Symbol**	**Chitral Bridge**	**Bannu Bridge**	**Unit**	**Notes / Visual Reference**
Bridge Identification		Chitral Bridge	Bannu Road Bridge		From Figure 4
Design Life	-	75	75	years	
Span Length	L	35	30	m	Supported span
Girder Concrete Strength					From Table 3
- At service state	-	35	35	MPa	
- At prestressing	-	28	28	MPa	
Deck Slab Concrete Strength	-	35	35	MPa	
Reliability Index (β)	-	2.51	5.6	-	From Table 4, via FORM method
Mean Applied Load	μ_0	6,132.34	6,132.34	kN-m	From WIM data
Standard Deviation of	σ_0	3,358	3,358	kN-m	

Load					
Coefficient of Variation (Load)	V_0	0.195 (19.5%)	0.195 (19.5%)	-	σ_0 / μ_0
Nominal Resistance	R_n	15,000	20,700	kN-m	Design value
Bias Factor of Resistance	λ_r	1.05	1.05	-	
Coefficient of Variation (Resistance)	V_r	0.075 (7.5%)	0.075 (7.5%)	-	Material variability
Girder Geometry:					From Figure 5 and Table 5
Top Flange Width	W1gir	800	900	mm	
Top Flange Thickness	T1gir	205	130	mm	
1st Triangle Width (Top)	W2gir	310	250	mm	
1st Triangle Height (Top)	T2gir	155	70	mm	
2nd Triangle Width (Top)	W3gir	100	100	mm	
2nd Triangle Height (Top)	T3gir	100	100	mm	
Middle Web Width	W4gir	180	200	mm	
Middle Web Height	T4gir	1,140	1,350	mm	
Triangle (Bottom) Width	W5gir	210	200	mm	
Triangle (Bottom) Height	T5gir	210	200	mm	
Bottom Flange Width	W6gir	600	600	mm	
Bottom Flange Thickness	T6gir	290	250	mm	

5 Conclusions

1. Pakistan's actual truck traffic has significantly different axle weights, axle configurations, and GVW than the values specified by the NHA Legal Load limits.
2. The load effects caused by actual truck traffic are much higher in some cases and much lower than those caused by live load models of the PHB Code and AASHTO Specification. Thus, bridges may be significantly overstressed, which may reduce their design life.
3. The safety index 'β' is considerably below or above the target value for both shear and moment. Hence, the existing live load model of the PHB Code and NHA legal limits are not accurate representations of Pakistan's actual truck traffic.

Recommendations

1. The existing live load model of the PHB Code does not accurately represent Pakistan's actual truck traffic; therefore, the Live load model needs to be revised and developed according to the actual truck traffic in Pakistan.
2. More stringent NHA legal load limits may be enforced.
3. Based on this study, it is recommended that reliability analyses of more bridges be carried out, and a new live load model may be developed if a similar lower safety level is found in those cases.

Author contributions

Hamza Shams Conceptualization, Methodology, Validation, Formal analysis, Investigation, Data curation, Writing—original draft preparation, Writing—review and editing, Yanjun QIU Supervision, Review and editing, Project administration, Funding acquisition, Muhammad Kashif Writing and editing, Hanif Ullah Writing Review and editing, Hamid Abdrhman Writing and editing, Jianfeng FU, Enhui Yang funding acquisition.

Conflicts of interest

The authors declare no conflict of interest.

Acknowledgment

This research was supported jointly by a research project "Distress identification and design optimization of concrete bridge deck paving in mountainous areas" from Sichuan Mianjiu Expressway CO., LTD (No.KY3) and NSFC of 52178438.

References

[1] Nowak, Andrzej S., and Kevin R. Collins. *Reliability of structures*. CRC press, 2012.

[2] Zhao, Zhisong, Nasim Uddin, and Eugene J. O'Brien. "Bridge weigh-in-motion algorithms based on the field calibrated simulation model." *Journal of Infrastructure Systems* 23.1 (2017): 04016021.

[3] Huff, Tim. *LRFD Bridge Design: Fundamentals and Applications*. CRC Press, 2022.

[4] Nowak, Andrzej S. *Calibration of LRFD bridge design code*. No. Project C12-33 FY'88-'92. 1999.

[5] Caprani, Colin C., Eugene J. OBrien, and Alessandro Lipari. "Long-span bridge traffic loading based on multi-lane traffic micro-simulation." *Engineering Structures* 115 (2016): 207-219.

[6] Melchers, Robert E., and André T. Beck. "Structural Reliability Analysis and Prediction."

[7] Hafeez, Imran. "49. Analysis of Truck Traffic using Weight-In-Motion (WIM) Data." *1ST INTERNATIONAL CONFERENCE ON RECENT ADVANCES IN CIVIL AND EARTHQUAKE ENGINEERING (ICCEE-2021)–OCT 08, 2021*. 2021.

[8] Ghosh, Jayadipta, Colin C. Caprani, and Jamie E. Padgett. "Influence of traffic loading on the seismic reliability assessment of highway bridge structures." *Journal of Bridge Engineering* 19.3 (2014): 04013009.

[9] Fan, Ziyuan, et al. "Fatigue reliability analysis for suspenders of a long-span suspension bridge considering random traffic load and corrosion." *Structures*. Vol. 56. Elsevier, 2023.

[10] https://www.scribd.com/document/33818701/Code-of-Practice-Highway-Bridges-1967

[11] Zheng, Xilong, et al. "Static and dynamic performance analysis of cable-stayed bridges with cables damaged fire." *Buildings* 14.4 (2024): 884.
[12] Žnidarič, Aleš, Maja Kreslin, and Jan Kalin. "Weigh-in-motion and traffic load monitoring." *Fact Sheet WG* (2016): 2-9.
[13] Bashir, Muhammad Mahtab. "Bahauddin Zakariya University Multan (Pakistan)." (2023).
[14] Faber, Michael H., Dimitri V. Val, and Mark G. Stewart. "Proof load testing for bridge assessment and upgrading." *Engineering structures* 22.12 (2000): 1677-1689.
[15] Bhattacharya, Baidurya. "Risk and reliability in bridges." *Innovative Bridge Design Handbook*. Butterworth-Heinemann, 2022. 169-213.
[16] Rasheed, Abdur, et al. "Structural reliability analysis of superstructure of highway bridges on China-Pakistan Economic Corridor (CPEC): A case study." *Journal of Structural Integrity and Maintenance* 3.3 (2018): 197-207.
[17] Deng, Yang, et al. "Serviceability assessment for long-span suspension bridge based on deflection measurements." *Structural Control and Health Monitoring* 25.11 (2018): e2254.
[18] Ghosh, Jayadipta, and Piyush Sood. "Consideration of time-evolving capacity distributions and improved degradation models for seismic fragility assessment of aging highway bridges." *Reliability Engineering & System Safety* 154 (2016): 197-218.
[19] Ticona Melo, Ladislao R., et al. "Dynamic response of a railway bridge to heavy axle-load trains considering vehicle–bridge interaction." *International Journal of Structural Stability and Dynamics* 18.01 (2018): 1850010.
[20] Matua, Moses Trevor Mandela. *Framework for the assessment of reliability in existing RC bridges in South Africa using visual inspection data*. Diss. Stellenbosch University, 2024.
[21] Ede, Anthony, et al. "Failure trend of transport infrastructure in developing nations: Cases of bridge collapse in Nigeria." *IOP conference series: materials science and engineering*. Vol. 640. No. 1. IOP Publishing, 2019.
[22] Sivakumar, B., Michel Ghosn, and E. Senturk. "Development of LRFR provisions for emergency vehicles." *Bridge Maintenance, Safety, Management, Life-Cycle Sustainability and Innovations*. CRC Press, 2021. 528-534.
[23] Wang, Ruoqi, John Leander, and Raid Karoumi. "Fatigue reliability assessment of steel bridges considering spatial correlation in system evaluation." *Structure and Infrastructure Engineering* 19.2 (2023): 254-268.
[24] Nowak, Andrzej S., and Maria M. Szerszen. "Structural reliability as applied to highway bridges." *Progress in Structural Engineering and Materials* 2.2 (2000): 218-224.
[25] Ellingwood, Bruce, et al. "Development of methods of structural reliability." *Structural Safety* 113 (2025): 102474.

GUIDE FOR AUTHORS

In the journal *Building Materials and Structures*, the submission and review processes take place electronically. Manuscripts are submitted electronically (online) on the website **https: //** www.dimk.rs. The author should register first, then log in and finally submit the manuscript which should be in the form of editable files (e.g. Word) to enable the typesetting process in journal format. All correspondence, including Editor´s decision regarding required reviews and acceptance of manuscripts, take place via e-mail.

TYPES OF ARTICLES

The following types of articles are published in *Building Materials and Structures:*

Original scientific article. It is the primary source of scientific information, new ideas and insights as a result of original research using appropriate scientific methods. The results are presented briefly, but in a way to enable readers to assess the results of experimental or theoretical/numerical analyses, so that the research can be repeated and yield with the same or results within the limits of tolerable deviations.

Review article. It presents the state of science in particular area as a result of methodically systematized, analyzed and discussed reference data. Only critical review manuscripts will be considered as providing novel perspective and critical evaluation of the topics of interest to broader BMS readership.

Preliminary report. Contains the first short notifications of research results without detailed analysis, i.e. it is shorter than original research paper.

Technical article. Reports on the application of recognized scientific achievements of relevance to the field of building materials and structures. Contain critical analysis and recommendations for adaption of the research results to practical needs.

Projects Notes. Project Notes provide a presentation of a relevant project that has been built or is in the process of construction. The original or novel aspects in design or construction should be clearly indicated.

Discussions. Comment on or discussion of a manuscript previously published in *Building Materials and Structures*. It should be received by the Editor-in-Chief within six months of the online publication of the manuscript under discussion. Discussion Papers will be subject to peer review and should also be submitted online. If Discussion Paper is selected for publication the author of the original paper will be invited to respond, and Discussion Paper will be published alongside any response that the author.

Other contributions

Conference Reports. Reports on major international and national conferences of particular interest to *Building Materials and Structures*. Selected and/or awarded papers from the ASES Conferences are published in Special issues.

Book Reviews. Reviews on new books relevant to the scope of *Building Materials and Structures*.

PREPRINTS

These are the author's own write-up of research results and analysis that has not been peer reviewed, nor had any other value added to it by a publisher (such as formatting, copy-editing, technical enhancements and the like). Authors can share their preprint anywhere at any time. If accepted for publication, we encourage authors to link from the preprint to their formal publication via its Digital Object Identifier (DOI). Preprints should not be added to or enhanced in any way in order to appear more like, or to substitute for, the final versions of articles.

MANUSCRIPT STRUCTURE

The manuscript should be typed one-sided on A4 sheets. Page numbers should be included in the manuscript and the text should be single spaced with **consecutive line numbering** - these are essential peer review requirements. The figures and tables included in the single file should be placed next to the relevant text in the manuscript. The corresponding captions should be placed directly below the figure or table. If the manuscript contains Supplementary material, it should also be submitted at the first submission of the manuscript for review purposes.

There are no strict rules regarding the structure of the manuscript, but the basic elements that it should contain are: Title page with the title of the manuscript, information about the authors, abstract and keywords, Introduction, Materials / Methods, Results and Conclusions.

The front page

The front page contains the title of the manuscript which should be informative and concise; abbreviations and formulas should be avoided.

Information about the authors are below the title; after the author's name, a superscript number is placed indicating his/her affiliation, which is printed below the author's name, and before the abstract. It is obligatory to mark the corresponding author with superscript *) and provide his/her e-mail address. The affiliation should contain the full name of the institution where the author performed the research and its address.

Abstract

Abstract should contain 150-200 words. Motivation and objective of the conducted research should be presented; main results and conclusions should be briefly stated as well. References and abbreviations should be avoided.

Keywords

Keywords (up to 10) should be listed immediately after the abstract; abbreviations should be used only if they are generally accepted and well-known in the field of research.

Division into chapters

The manuscript should be divided into chapters and sub-chapters, which are hierarchically numbered with Arabic numbers. The headings of chapters and sub-chapters should appear on their own separate lines.

At the end of the manuscript, and before the references, it is obligatory to list the following statements:

CRediT authorship contribution statement

For transparency, we require corresponding authors to provide co-author contributions to the manuscript using the relevant CRediT roles. The CRediT taxonomy includes 14 different roles describing each contributor's specific contribution to the research output. The roles are: Conceptualization; Data curation; Formal analysis; Funding acquisition; Investigation; Methodology; Project administration; Resources; Software; Supervision; Validation; Visualization; Roles/Writing - original draft; and Writing - review & editing. Note that not all roles may apply to every manuscript, and authors may have contributed through multiple roles.

Declaration of competing interest

Corresponding authors, on behalf of all the authors of a submission, must disclose any financial and personal relationships with other people or organizations that could inappropriately influence their work. Examples of potential conflicts of interest include employment, consultancies, stock ownership, honoraria, paid expert testimony, patent applications/registrations, and grants or other funding. All authors, including those *without* competing interests to declare, should provide the relevant information to the corresponding author (which, where relevant, may specify they have nothing to declare).

Declaration of generative AI in scientific writing

This guidance only refers to the writing process, and not to the use of AI tools to analyze and draw insights from data as part of the research process. Where authors use generative artificial intelligence (AI) and AI- assisted technologies in the writing process, authors should only use these technologies to improve readability and language. Applying the technology should be done with human oversight and control, and authors should carefully review and edit the result, as AI can generate authoritative-sounding output that can be incorrect, incomplete or biased. AI and AI-assisted technologies should not be listed as an author or co-author, or be cited as an author. Authorship implies responsibilities and tasks that can only be attributed to and performed by humans. Authors should disclose in their manuscript the use of AI and AI- assisted technologies in the writing process by following the instructions below. A statement will appear in the published work. Please note that authors are ultimately responsible and accountable for the contents of the work.

Disclosure instructions

Authors must disclose the use of generative AI and AI-assisted technologies in the writing process by adding a statement at the end of their manuscript in the core manuscript file, before the References list. The statement should be placed in a new section entitled 'Declaration of Generative AI and AI-assisted technologies in the writing process'.

Statement: During the preparation of this work the author(s) used [NAME TOOL / SERVICE] in order to [REASON]. After using this tool/service, the author(s) reviewed and edited the content as needed and take(s) full responsibility for the content of the publication.
This declaration does not apply to the use of basic tools for checking grammar, spelling, references etc. If there is nothing to disclose, there is no need to add a statement.

Acknowledgments

State the institutions and persons who financially or in some other way helped the presented research. If the research was not supported by others, it should also be stated in this part of the manuscript.

Appendices

The manuscript may have appendices. If there is more than one appendix, they are denoted by A, B, etc. Labels of figures, tables and formulas in appendices should contain the label of the appendix, for example Table A.1, Figure A.1, etc.

ABBREVIATIONS

All abbreviations should be defined where they first appear. Consistency of abbreviations used throughout the text should be ensured.

MATH FORMULAE

Formulae should be in the form of editable text (not in the format of figures) and marked with numbers, in the order in which they appear in the text. The formulae and equations should be written carefully takinginto account the indices and exponents. Symbols in formulae should be defined in the order they appear, right below the formulae.

FIGURES

- figures should be made so that they are as uniform in size as possible and of appropriate quality for reproduction;
- the dimensions of the figures should correspond to the format of the journal: figures with a width approximately equal to the width of 1 column (± 80 mm width), width of 2 columns (± 170 mm width) or width of 1.5 columns (± 130 mm width);
- figures should be designed so that their size is not disproportionately large in relation to the content;
- the text on the figures should be minimal and the font used should be the same on all figures (Arial, Times New Roman, Symbol);
- figures should be placed next to the appropriate text in the manuscript and marked with numbers in the order in which they appear in the text;
- each figure should have a caption that is placed below the figure - the caption should not be on the figure itself.

In cases of inadequate quality of reproduction, the author should be required to submit figures as separate files. In this case, the figure should be saved in TIFF (or JPG) format with a minimum resolution of 500 dpi.

TABLES

- tables should be in the form of editable text (not in the format of figures);
- tables should be placed next to the appropriate text in the manuscript and marked with numbers in the order in which they appear in the text;
- each table should have a caption that is placed below the table;
- the tables should not show the results that are already presented elsewhere in the manuscript - duplicating the presentation of results should be avoided;
- tables are without vertical lines as boundaries between cells and shading cells.

REFERENCES

Citation in the text

Each reference cited in the text should be in the reference list (and vice versa). It is not recommended to list unpublished results or personal communications in the reference list, but they can be listed in the text. If they are still listed in the reference list, the journal style references are used, with 'Unpublished results' or 'Personal communication' instead of the date of publication. Citing a reference as ‘in press’ means that it is accepted for publication.

Web references

Web references are minimally listed with the full URL and the date when the site was last accessed. These references can be included in the reference list, but can also be given in a separate list after the reference list.

Reference style

In text: References are given in the text by a number in square brackets in the order in which they appear in the text. Authors may also be referred to directly, but the reference number should always be given.

In reference list: References marked with a number in square brackets are sorted by numbers in the list.

Examples

Reference to a journal publication:

[1] V.W.Y. Tam, M. Soomro, A.C.J. Evangelista, A review of recycled aggregate in concrete applications (2000-2017), Constr. Build. Mater. 172 (2018) 272-292. https://doi.org/10.1016/j.conbuildmat.2018.03.240.

Reference to a book:

[3] A.H. Nilson, D. Darwin, C.W. Dolan, Design of Concrete Structures, thirteenth ed., Mc Graw Hill, New York, 2004.

Reference to a chapter in an edited book:

[4] J.R. Jimenez, Recycled aggregates (RAs) for roads, in: F Pacheco-Torgal, V.W.Y. Tam, J.A. Labrincha, Y. Ding, J. de Brito (Eds.), Handbook of recycled concrete and demolition waste, Woodhead Publishing Limited, Cambridge, UK, 2013, pp. 351–377.

Reference to a website:

[5] WBCSD, The Cement Sustainability Initiative, World. Bus. Counc. Sustain. Dev. http://www.wbcsdcement.org.pdf/CSIRecyclingConcrete-FullReport.pdf, 2017 (accessed 7 July 2016).

SUPPLEMENTARY MATERIAL

Supplementary material such as databases, detailed calculations and the like can be published separately to reduce the workload. This material is published ‘as received’ (Excel or PowerPoint files will appear as such online) and submitted together with the manuscript. Each supplementary file should be given a short descriptive title.

ETHICS IN PUBLISHING

Authors are expected to respect intellectual and scientific integrity in presentation of their work. The journal publishes manuscripts that have not been previously published and are not in the process of being considered for publication elsewhere. All co-authors as well as the institution in which the research was performed should agree to the publication in the journal.
Authors are expected to submit completely original research; if the research of other researchers is used, it should be adequately cited. Authors who wish to include in their manuscript images, tables or parts of text that have already been published somewhere, should obtain permission from the Copyright owner and provide a proof in the process of submitting the manuscript. All material for which there is no such evidence will be considered the original work of the author. To determine the originality of the manuscript, it can be checked using the Crossref Similarity Check service. For more information, please see our Ethics and Malpractice Statement.

The Journal and Publishers imply that all authors, as well as responsible persons of the institute where the research was performed, agreed with the content of the submitted manuscript before submitting it. The Publishers will not be held legally responsible should there be any claims for compensation.

PEER REVIEW

This journal uses a single blind review process, which means that the authors do not know the names of the reviewers, but the reviewers know who the authors are. In the review process, the Editor-in-Chief first assesses whether the contents of the manuscript comply with the scope of the journal. If this is the case, the paper is sent to at least two independent experts in the field, with the aim of assessing its scientific quality and making recommendation regarding publication. If the manuscript needs to be revised, the authors are provided with the reviewers' remarks. The authors are obliged to correct the manuscript in accordance with the remarks, submit the revised manuscript and a special file with the answers to the reviewers within the given deadline. The final decision, whether the paper will be published in journal or not, is made by the Editor-in-Chief.

AFTER ACCEPTANCE

Once accepted for publication, the manuscript is set in the journal format. Complex manuscript is sent to the authors in the form of proof, for proof reading. Then, authors should check for typesetting errors, and whether the text, images, and tables are complete and accurate. Authors are asked to do this carefully, as subsequent corrections will not be considered. In addition, significant changes to the text and authorship at this stage are not allowed without the consent of the Editor-in-Chief. After online publication, changes are only possible in the form of Erratum which will be hyperlinked to manuscript.

COPYRIGHT

Authors retain copyright of the published papers and grant to the publisher the non-exclusive right to publish the article, to be cited as its original publisher in case of reuse, and to distribute it in all forms and media.

The published articles will be distributed under the Creative Commons Attribution ShareAlike 4.0 International license (CC BY-SA). It is allowed to copy and redistribute the material in any medium or format, and remix, transform, and build upon it for any purpose, even commercially, as long as appropriate credit is given to the original author(s), a link to the license is provided, it is indicated if changes were made and the new work is distributed under the same license as the original.

Users are required to provide full bibliographic description of the original publication (authors, article title, journal title, volume, issue, pages), as well as its DOI code. In electronic publishing, users are also required to link the content with both the original article published in *Building Materials and Structures* and the license used.

Authors are able to enter into separate, additional contractual arrangements for the non-exclusive distribution of the journal's published version of the work (e.g., post it to an institutional repository or publish it in a book), with an acknowledgement of its initial publication in this journal.

OPEN ACCESS POLICY

Journal *Building Materials and Structures* is published under an Open Access license. All its content is available free of charge. Users can read, download, copy, distribute, print, search the full text of articles, as well as to establish HTML links to them, without having to seek the consent of the author or publisher.
The right to use content without consent does not release the users from the obligation to give the credit to the journal and its content in a manner described under *Copyright*.

Archiving digital version

In accordance with law, digital copies of all published volumes are archived in the legal deposit library of the National Library of Serbia in the Repository of SCIndeks - The Serbian Citation Index as the primary full text database.

Cost collection to authors

Journal Building Materials and Structures does not charge authors or any third party for publication. Both manuscript submission and processing services, and article publishing services are free of charge. There are no hidden costs whatsoever.

DISCLAIMER

The views expressed in the published works do not express the views of the Editors and the Editorial Staff. The authors take legal and moral responsibility for the ideas expressed in the articles. Publisher shall have no liability in the event of issuance of any claims for damages. The Publisher will not be held legally responsible should there be any claims for compensation.

Financial support

MINISTRY OF EDUCATION, SCIENCE AND TECHNOLOGICAL DEVELOPMENT OF REPUBLIC OF SERBIA

INSTITUTE FOR TESTING OF MATERIALS-IMS INSTITUTE, BELGRADE

SERBIAN CHAMBER OF ENGINEERS

INŽENJERSKA KOMORA SRBIJE

Ringlock

Doka modularni sistem skela.

Bezbedno i efikasno rešenje za skele. Široka oblast primena.

doka

PROVIDING ATPAC COMPLETE SCAFFOLDING SOLUTIONS

Pristupne skele

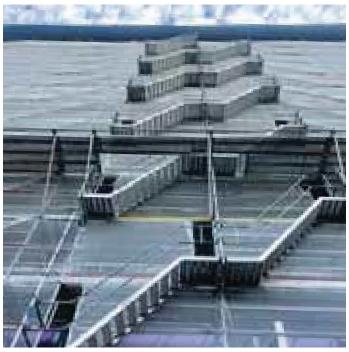

Skele za stambene objekte

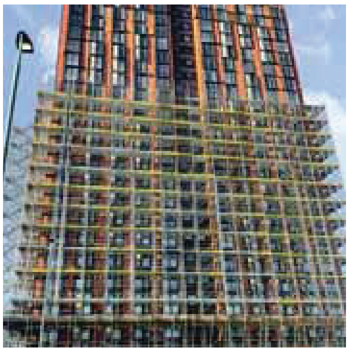

Skele za poslovne objekte

Stepenišni toranj

Doka Serb d.o.o. | Svetogorska 4 | 22310 Šimanovci | Srbija | **T** +381 (0)22 400 100 | serb@doka.com | **www.doka.com/rs**

INSTITUT IMS AD
BEOGRAD

CENTAR ZA PUTEVE I GEOTEHNIKU

U okviru centra posluju odeljenja za geotehniku, nadzor i terenska ispitivanja, projektovanje saobraćajnica, laboratorija za puteve i geotehniku. Značajna aktivnost centra usmerena je ka terenskim i laboratorijskim geološko - geotehničkim istraživanjima i ispitivanjima terena za potrebe izrade projekno - tehničke dokumentacije, za različite faze i nivoe projektovanja objekata visokogradnje, niskogradnje, saobraćaja i hidrogradnje, kao i za potrebe prostornog planiranja i zaštite životne sredine. Stručni nadzor, kontrola kvaliteta tokom građenja, rekonstrukcije i sanacije objekata različite namene, izrada studija, ekspertiza, konsultantske usluge, kompletan konsalting u oblasti geotehničkog inženjeringa, neke su od delatnosti centra.

Ispitivanje šipova

- **SLT metoda (Static load test)**
- **DLT metoda (Dynamic load test)**
- **PDA metoda (Pile driving analysis)**
- **PIT (SIT) metoda (Pile (Sonic) integrity testing)**
- **CSL - Crosshole Sonic Logging**

ИМС IMS INSTITUT IMS AD BEOGRAD

- **<u>Ispitivanje šipova</u>**
  - **<u>Geotehnička istraživanja i ispitivanja – in situ</u>**
    - **<u>Laboratorija za puteve i geotehniku</u>**
      - **<u>Projektovanje puteva i sanacija klizišta</u>**
        - **<u>Nadzor</u>**

PUT INŽENJERING

Put inženjering d.o.o punih 25 godina radi kao specijalizovano preduzeće za izgradnju infrastrukture u niskogradnji i visokogradnji, kao i proizvodnjom kamenog agregata i betona. Preduzeće se bavi i transportom, uslugama građevinske mehanizacije i specijalne opreme.

Za spravljanje betona koristimo drobljeni krečnjački agregat sa našeg kamenoloma, deklarisanih frakcija, kontrolisane vlažnosti. Kompletan proces proizvodnje i kontrole kvaliteta vršimo prema važećim standardima.

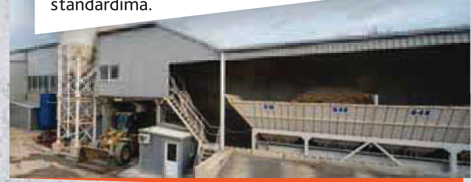

Kao generalni izvođač radova, vršimo koordinaciju svih učesnika na projektu, planiranje, praćenje i nabavku materijala, kontrolu kvaliteta izvedenih radova, poštujući zadate vremenske rokove i finansijski okvir investitora.

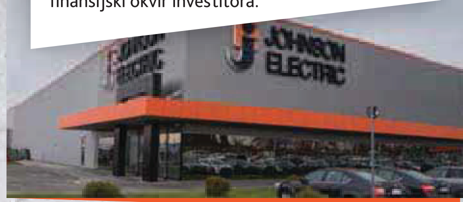

Obradu armature vršimo brzo, stručno i kvalitetno, sa kompjuterskom preciznošću i dimenzijama po projektu.

Osnovi princip našeg poslovanja zasniva se na individualnom pristupu svakom klijentu i pronalaženje najoptimalnijeg rešenja za njegove transportne i logističke potrebe.

Koristeći inovativne tehnike i kvalitetan građevinski materijal iz sopstvenih resursa, spremni smo da odgovorimo na mnoge zahteve naših klijenata iz oblasti niskogradnje.

Naša kompanija u oblasti visokogradnje primenjuje sistem prefabrikovnih betonskih elemenata koji u odnosu na klasičnu gradnju ima brojne prednosti.

Usluge građevinskom mehanizacijom vršimo tehnički ispravnim mašinama, sa potrebnim sertifikatima kako za rukovaoce građevinskim mašinama tako i za same mašine.

Osnovna prednost prefabrikovane konstrukcije jeste brzina kojom konstrukcija može biti projektovana, proizvedena, transportovana i namontirana.

Prednapregnute šuplje ploče su konstruktivni elementi visokog kvaliteta, proizvedeni u fabrički kontrolisanim uslovima.

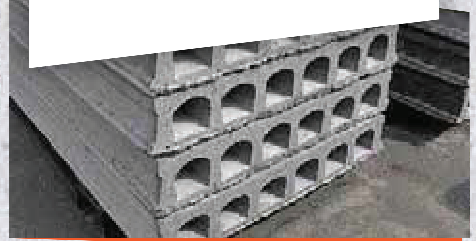

Raspolažemo opremom i mašinama za sve zemljane radove, kipere i dampere za rad u teškim terenskim uslovima, automiksere i pumpe za beton, autodizalice, podizne platforme.

Izvodimo hidrograđevinske radove u izgradnji kanalizacionih mreža za odvođenje atmosferskih, otpadnih i upotrebljenih voda, izvođenjem hidrograđevinskih radova u okviru regulacije rečnih tokova, kao i izvođenjem hidrotehničkih objekata.

Izrađujemo betonske "New Jersey profile" koji se u svetu koriste za preusmeravanje saobraćaja i zaštitu pešaka u toku izgradnje puta, kao i Betonblock sistem betonskih blokova.

Sakupljanje i privremeno skladištenje otpada vršimo našim specijalizovanim vozilima i deponujemo na našu lokaciju sa odgovarajućom dozvolom. Kapacitet mašine je 250 t/h građevinskog neopasnog otpada.

Površinski kop udaljen je 35 km od Niša. Savremene drobilice, postrojenje za separaciju i sejalica efikasno usitnjavaju i razdvajaju kamene agregate po veličinama. Tehnički kapacitet trenutne primarne drobilice je 300 t/h.

Uslugu transporta vršimo automikserima, kapaciteta bubnja od 7 m³ do 10 m³ betonske mase. Za ugradnju betona posedujemo auto-pumpu za beton, radnog učinka 150 m³/h, sa dužinom strele od 36 m.

NIŠ
Knjaževačka bb, 18000 Niš - Srbija
+381 18 215 355
office@putinzenjering.com

BEOGRAD
Jugoslovenska 2a, 11250 Beograd – Železnik
+381 11 25 81 111
beograd@putinzenjering.com

MOBECO

www.putinzenjering.com

MATEST
YOUR PARTNER IN TESTING

iT TECH

INELAS ERECO d.o.o

MATEST "iT TECH" KONTROLNA JEDINICA

JEDNA TEHNOLOGIJA MNOGO REŠENJA

IT Touch Techlogy je Matestov najnoviji koncept koji ima za cilj da ponudi inovativna i user-friendly tehnologiju za kontrolu i upravljanje najmodernijom opremom u domenu testiranja građevinskih materijala

Ova tehnologija je srž Matestove kontrolne jedinice, software baziran na Windows platformi i touch screen sistem koji je modularan, fleksibilan i obavlja mnoge opcije

iT TECH pokriva

| INOVATIVNOST
| INTERNET KONEKCIJA
| INTERFEJS SA IKONICAMA
| INDUSTRIJALNA TEHNOLOGIJA

SISTEM JEDNOG RAZMIŠLJANJA **JEDNOM SHVATIŠ - SVE TESTIRAŠ**

NAPREDNA TEHNOLOGIJA ISPITIVANJA ASFALTA

| GYROTRONIC - Gyratory Compactor
| ARC - Electromechanical Asphalt Roller Compactor
| ASC - Asphalt Shear Box Compactor
| SMARTRACKER^{tm} - Multiwheels Hamburg Wheel Tracker, DRY + WET test environment
| SOFTMATIC - Automatic Digital Ring & Ball Apparatus
| Ductilometers with data acquisition system

MULTIFUNKCIONALNI RAMOVI ZA TESTIRANJE

| CBR/Marshall digital machines
| Universal multispeed load frames
| UNITRONIC 50kN or 200kN Universal multipurpose compression/flexural and tensile frames

OPREMA ZA GEOMEHANIČKO ISPITIVANJE

| EDOTRONIC - Automatic Consolidation Apparatus
| SHEARLAB - AUTOSHEARLAB - SHEARTRONIC Direct / Residual shear testing systems
| Triaxial Load Frame 50kN

MIXMATIC - Automatic Programmable Mortar Mixer

INELAS ERECO D.O.O
Tošin bunar 274a, 11070 , Novi Beograd tel. +381 11 2284 574 email. info@inelasereco.rs

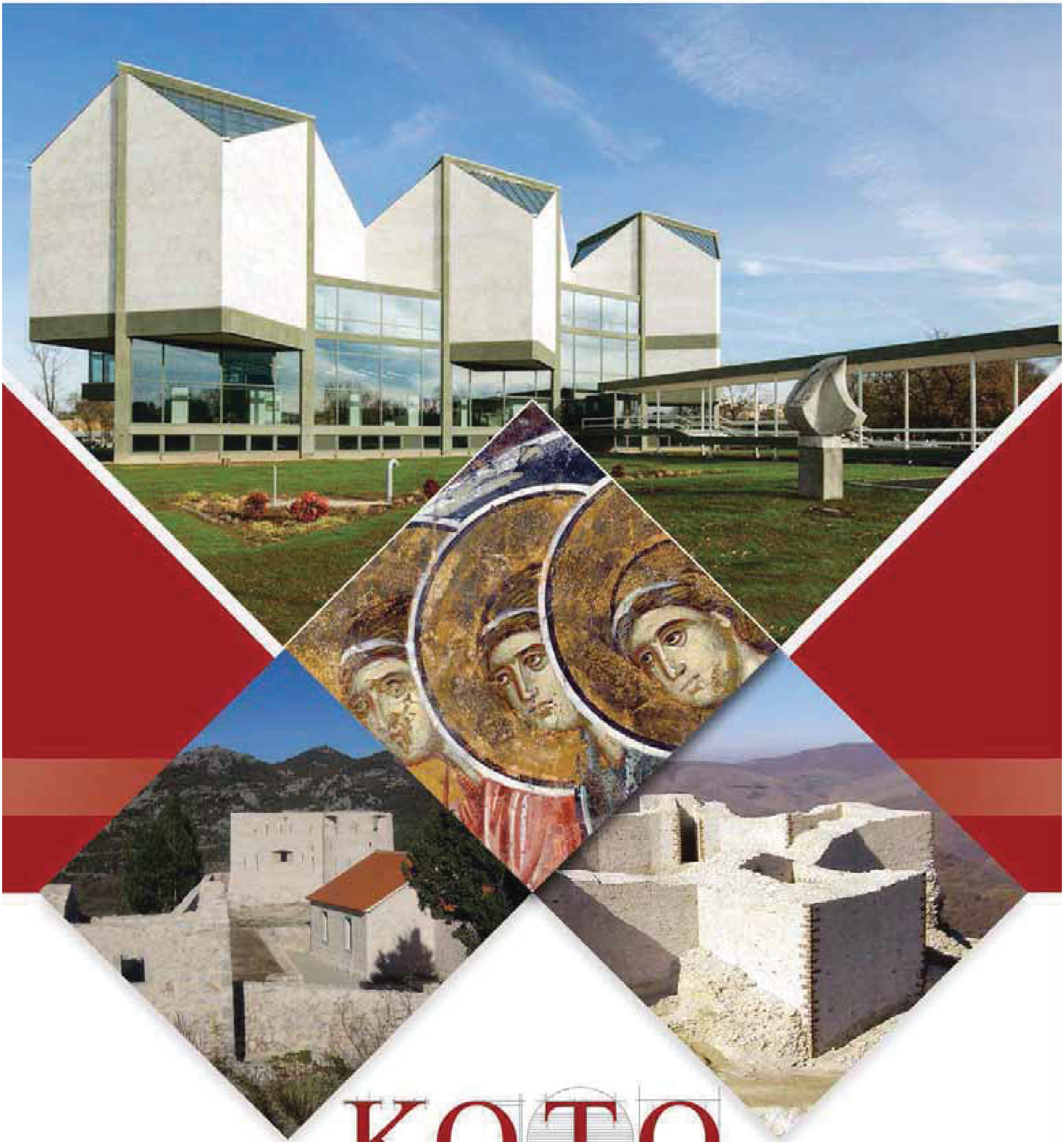

INNOVATIVE CONSTRUCTION TECHNOLOGIES

NOVKOL

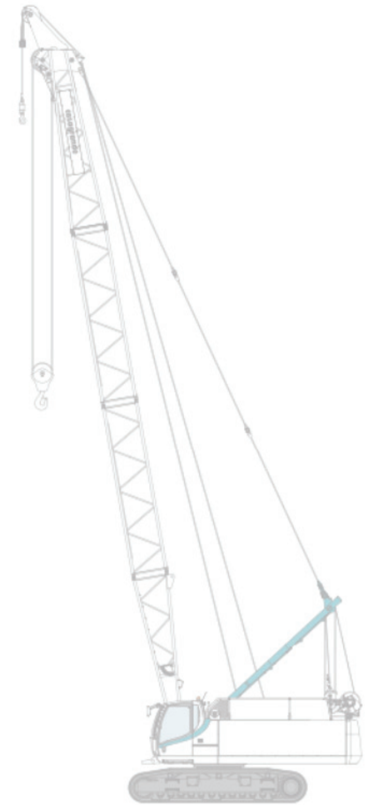

Samarska 6
(bivši Surčinski put 1k),
11077, Novi Beograd, Srbija

+381117129180
+381117129194
+381117129324
+381112607979
+381112607981

Fax:
+381117129183

office@novkol.co.rs
priprema@novkol.co.rs